

# Surface coating of materials for Hydroturbine applications

*Submitted in the partial fulfillment of the requirement for  
the award of the degree*

*Of*

**MASTER OF TECHNOLOGY**

*Under the supervision of Dr. VIVEK PANCHOLI*

**M.Tech. Project Thesis | 16<sup>th</sup> May, 2018**

**Preetika Baniwal 16544012**



**IIT ROORKEE**

## **CANDIDATE’S DECLARATION**

I hereby declare that the proposed work presented in this dissertation entitled “**Surface coating of materials for Hydroturbine applications**” is in partial fulfilment of the requirements for the award of the degree of **Master of Technology in Industrial Metallurgy**, submitted in the **Department of Metallurgical and Materials Engineering, Indian Institute of Technology Roorkee** is an authentic record of my own work carried out during the period of July 2017 to May 2018 under the supervision of **Dr. Vivek Pancholi**, Associate Professor, Department of Metallurgical and Materials Engineering, Indian Institute of Technology Roorkee, India.

The matter presented in this dissertation has not been submitted by me for the award of any other degree.

Dated:

Place:

(Preetika Baniwal)

## **CERTIFICATE**

This is to certify that the above statement made by the candidate is correct to the best of my knowledge and belief

Dr. Vivek Pancholi

Associate Professor

Metallurgical and Materials Engineering

Indian Institute of Technology-Roorkee

Roorkee-247667 (India)

## ACKNOWLEDGEMENT

I owe a thanks to a many people who helped and supported me during writing of this thesis.

My deepest thanks to my advisor Dr. Vivek Pancholi (Associate professor, IIT Roorkee) who guided me and corrected my various mistakes with attention and care. He has taken pain to go through the project and make necessary corrections as and when needed.

I express my thanks to the HOD of Department of Metallurgical and Materials Engineering Dr. Anjan Sil for his precious support.

My deep sense of gratitude to my colleagues and lab members Mr. Aniruth Malkar and Mr. Raja for their support, encouragement, guidance and for reviewing my work.

I would also thank my Institution and all the professors of Department without whom this project would have been a distant reality. I also extend my heartfelt thanks to my well-wishers.

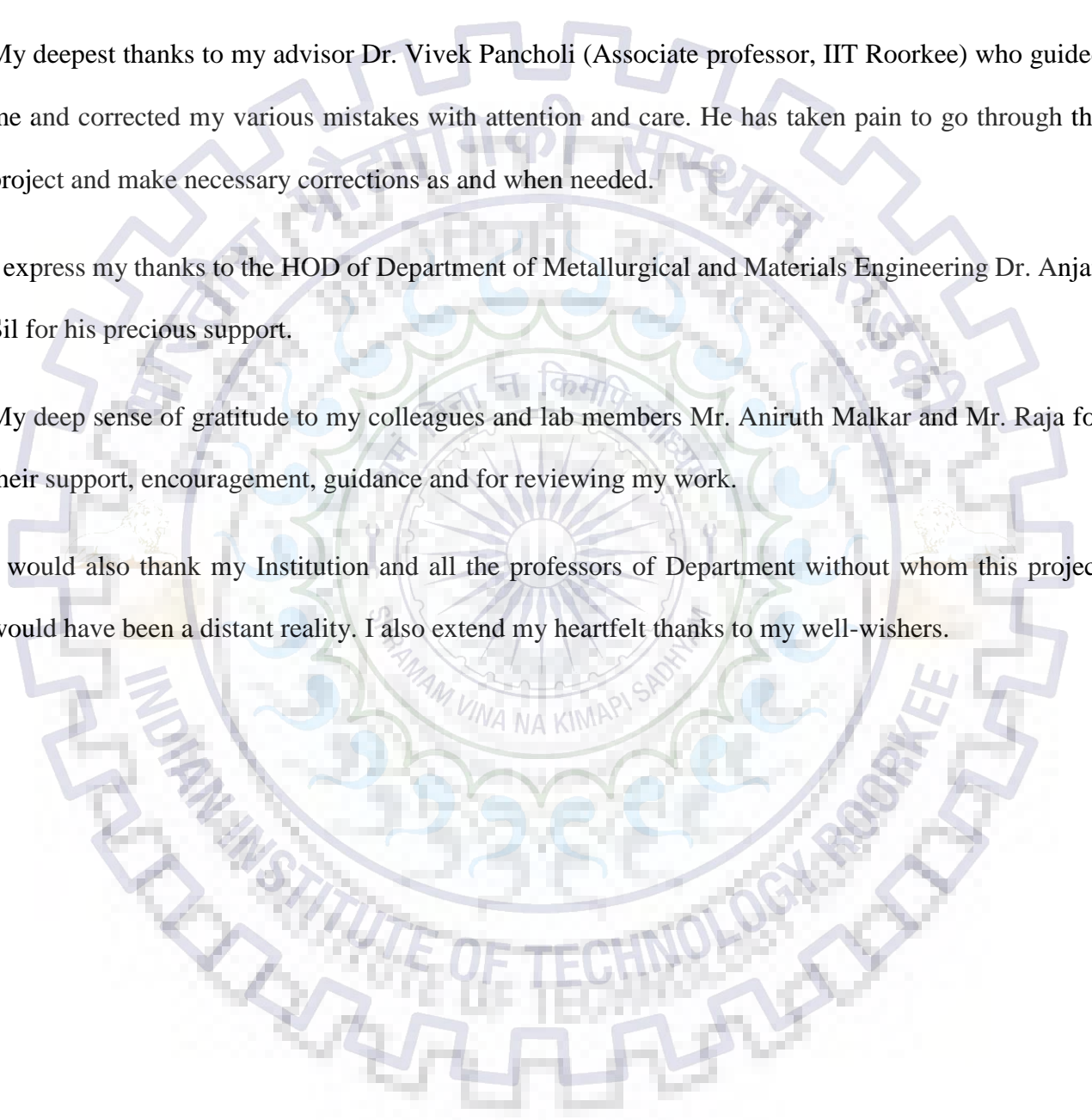


# Table of Contents

<b>1 INTRODUCTION</b> .....	<b>1</b>
1.1 WHY MARTENSITIC STAINLESS STEEL .....	2
1.2 WHY COATINGS.....	3
1.3 ASPECTS OF SILT EROSION.....	7
1.4 ASPECTS OF CAVITATION EROSION.....	7
<b>2 LITERATURE REVIEW</b> .....	<b>9</b>
2.1 TURBINE MATERIALS AND SURFACE MODIFICATIONS .....	10
2.2 THREE APPROACHES HAVE GENERALLY BEEN CONSIDERED .....	10
2.3 VARIOUS KINDS OF SURFACE TREATMENT PROCESSES.....	10
2.3.1 LASER HARDENING.....	10
2.3.2 NITRIDING .....	10
2.3.3 HIGH-VELOCITY OXY FUEL (HVOF) SPRAYING.....	10
2.4 EFFECT OF ANGLE OF IMPINGEMENT.....	11
2.4.1 COMPARISON BETWEEN NITRIDING AND HVOF COATING.....	12
2.5 PLASMA NITROCARBURIZING.....	14
2.6 CHARACTERISTICS OF A PROTECTIVE COATING UNDER HEAVY SILT CONDITIONS ARE.....	16
2.7 GAS NITRIDING.....	19
<b>3 OBJECTIVES AND PLAN OF WORK</b> .....	<b>20</b>
3.1 OBJECTIVE OF WORK.....	21
3.2 METHODOLOGY.....	22
<b>4. MATERIALS AND METHODS</b> .....	<b>25</b>
4.1 AISI 431 MARTENSITIC STAINLESS STEEL.....	25
4.2 SLURRY EROSION TEST.....	26
4.3 MICROHARDNESS TEST.....	27
<b>5 RESULTS AND DISCUSSIONS</b> .....	<b>31</b>
5.1 SEM ANALYSIS OF SILT. ....	31
5.2 MICROSTRUCTURE ANALYSIS... ..	32
5.3 SEM ANALYSIS OF MSS ERODED.....	33
5.4 SEM ANALYSIS OF MSS NITRIDED .....	34
5.5 SEM ANALYSIS OF NITRIDED LAYER .....	35
5.6 SEM ANALYSIS OF NITRIDED ERODED.....	37
5.7 XRD ANALYSIS.....	39
5.8 WEIGHT LOSS PLOT.....	41
5.9 MASS LOSS AND EROSION RATES.....	42
5.10 ROUGHNESS PROFILE AND MICROHARDNESS.....	43
<b>6 CONCLUSION</b> .....	<b>44</b>
<b>7 REFERENCES</b> .....	<b>45</b>

# LIST OF FIGURES

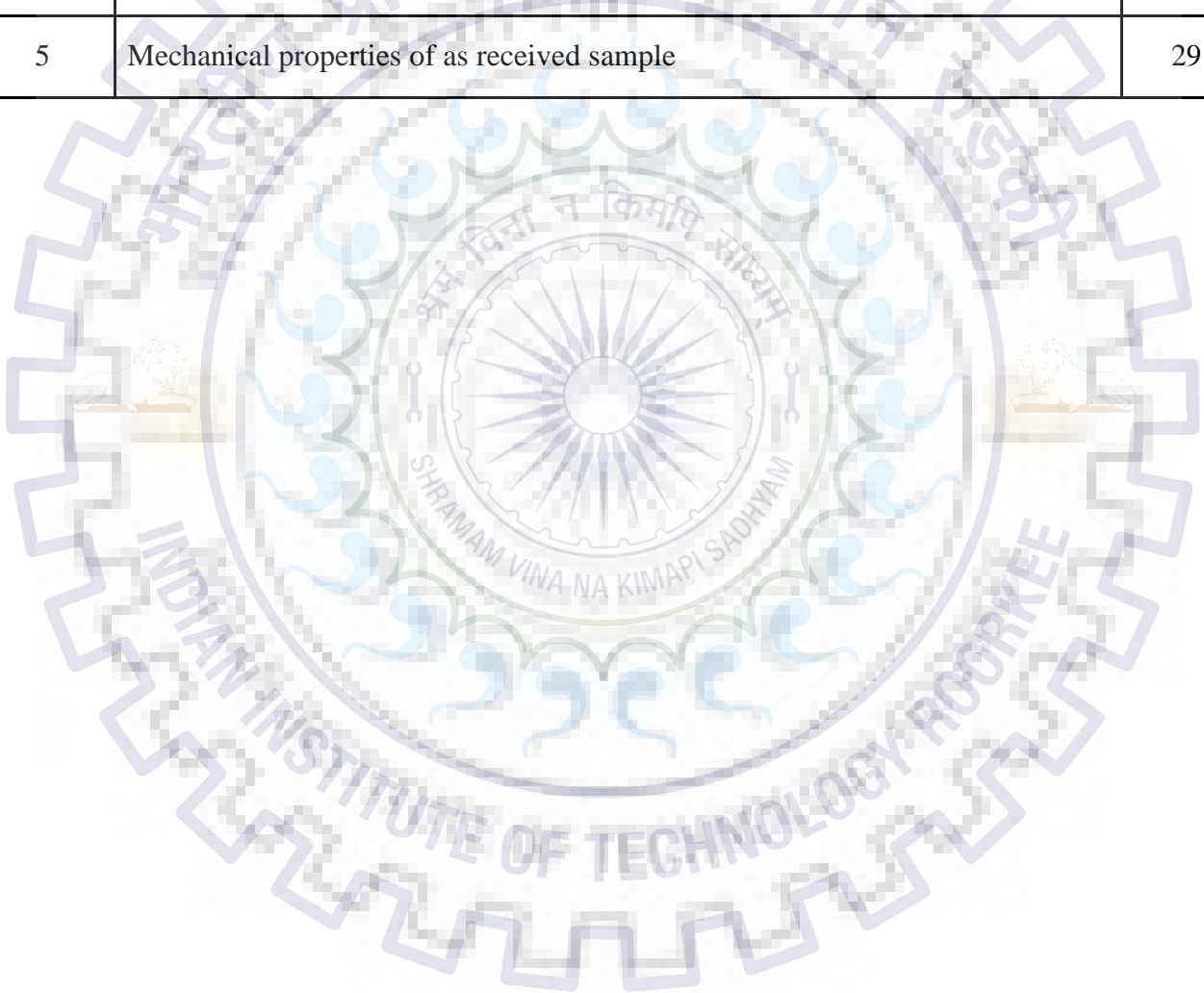
[1] Fig. (1) Runner blades showing cavitation erosive failure.....	3
[2] Fig (2) Turbine blade profile.....	4
[3] Fig (3) Turbine undergoing HVOF coating.....	6
[4] Fig (4) Various forms of Erosive wear mechanisms .....	7
[5] Fig (5) Damage in Pelton turbine needle due to pure sand and combined effect of sand and cavitation erosion.....	8
[6] Fig (6) Cross-sectional hardness distribution of (a) laser-hardened 13Cr-4Ni steels (b) pulsed-plasma nitrided 13Cr-4Ni steels.....	11
[7] Fig (7) The HVOF coating process being adopted on a spear of a Pelton turbine.....	11
[8] Fig (8) Erosion loss for modified steels and as received material at various angles of impingement.....	12
[9] Fig (9) Relationship between erosion rate and particle impingement energy.....	13
[10] Fig (10) Volume loss by cavitation erosion after removal of nitro carburized.....	15
[11] Fig (11) Vickers hardness as a function of depth below surface.....	15
[12] Fig. (12) Volume loss due to cavitation as a function of test duration.....	16
[13] Fig (13) Schematic diagram showing Nitriding process.....	17
[14] Fig (14) Micrograph shows both the compound layer and the underlying diffusion zone.....	18
[15] Fig (15) Spectroscopy results of as received.....	25
[16] Fig (16) Dimensions of as received sample.....	26
[17] Fig (17) samples obtained after wire cut EDM .....	26
[18] Fig (18) sand sieving pans.....	27
[19] Fig (19) sample holder of slurry testing machine.....	28
[20] Fig (20) slurry testing machine.....	28
[21] Fig (21) Microhardness Testing Machine.....	29
[22] Fig (22 a) SEM image of abrasive particles before test.....	31
[23] Fig (22 b) SEM image of abrasive particles after test.....	31
[24] Fig (23a) optical image of 16- 5 MSS depicting pro-eutectoid ferrite and chromium carbide.....	32
[25] Fig (23b) optical image of 16-5 MSS AISI 431 depicting lath needles and retained austenite.....	32
[26] Fig (24a) SEM of bare eroded specimen after test at 60 ° .....	33
[27] Fig (24b) SEM of bare eroded specimen after test at 60 ° .....	33
[28] Fig (24c) SEM of bare eroded specimen after test at 30 ° .....	33
[29] Fig (24d) SEM of bare eroded specimen after test at 30 ° .....	33
[30] Fig (25 a) SEM of nitrided layer.....	34
[31] Fig (25 b) SEM of nitrided layer depicting both zones.....	34
[32] Fig. (26a) Total case depth obtained.....	35
[33] Fig. (26b) SEM depicting diffusion zone and rest MSS.....	35

[34]	Fig. (26c) Chromium nitrides at grain boundaries.....	35
[35]	Fig. (26d) Back scatter image of expanded martensite.....	35
[36]	Fig (27a) back scatter image showing Grain boundary.....	36
[37]	Fig (27b) back scatter image showing chromium nitride.....	36
[38]	Fig (28a) SEM of nitrided eroded specimen after test at 60 °.....	37
[39]	Fig (28b) SEM of nitrided eroded specimen after test at 60 °.....	37
[40]	Fig (28c) SEM of nitrided eroded specimen after test at 30 °.....	37
[41]	Fig (28d) SEM of nitrided eroded specimen after test at 30 °.....	37
[42]	Fig (29a) X-ray diffraction patterns for non-nitrided.....	39
[43]	Fig (29b) X-ray diffraction patterns for nitrided specimens.....	39
[44]	Fig (30 a) X-ray diffraction patterns comparison b/w two.....	40
[45]	Fig (30 b) X-ray diffraction patterns showing peak shift b/w two specimens.....	40
[46]	Fig (31a) Wt. loss plot for non nitrided specimen.....	41
[47]	Fig (31b) Wt. loss plot for nitrided specimen.....	41
[48]	Fig (32a) wt. loss vs exposure time plot.....	42
[49]	Fig (32b) wt. loss vs angle of impingement.....	42
[50]	Fig (33a) Roughness profile.....	43
[51]	Fig (33b) Case hardness profile.....	43



## LIST OF TABLES

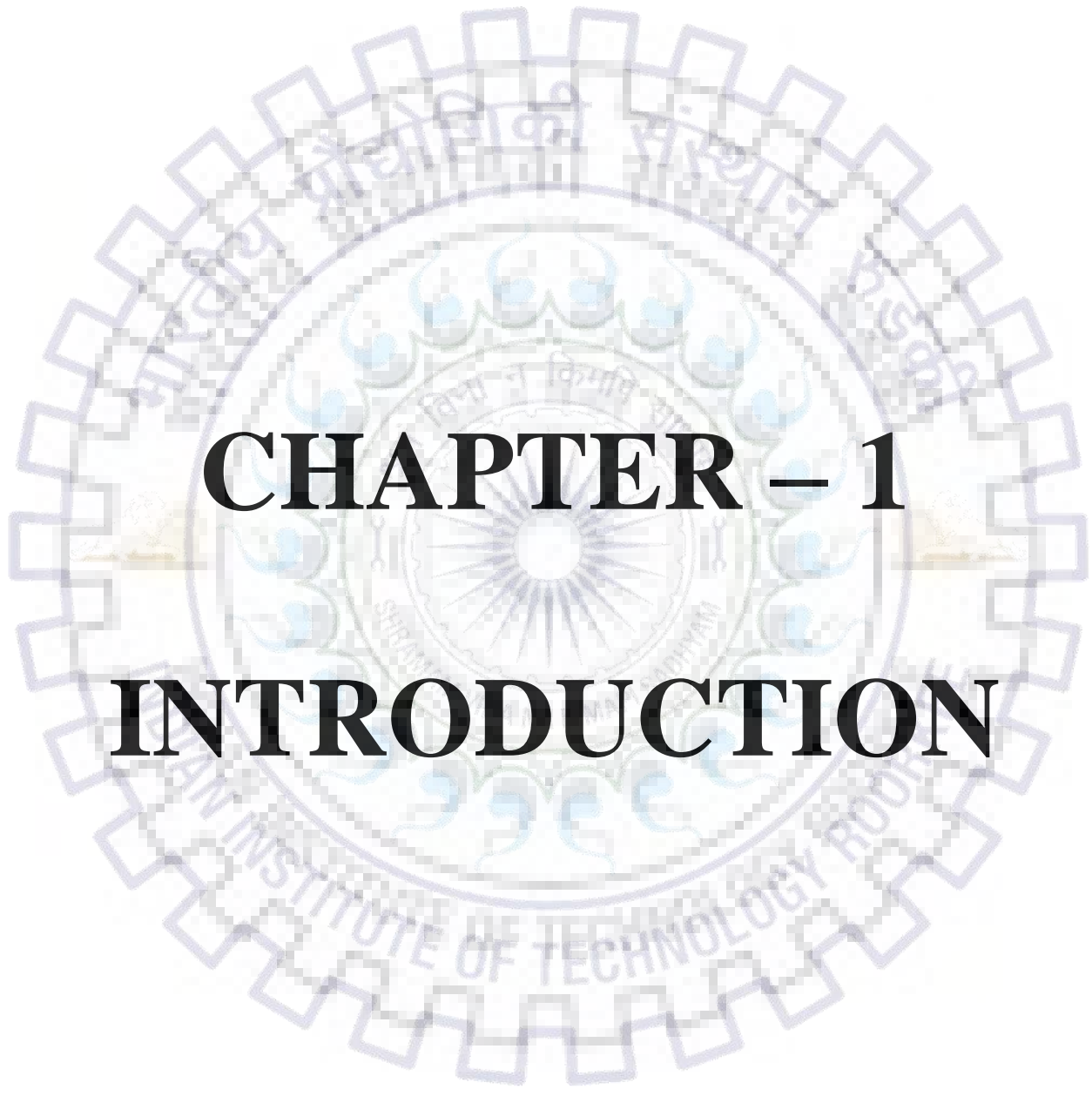
Table No.	Title	Page
1	Micro hardness of different coatings	13
2	Process parameters of plasma nitriding and gas nitriding	16
3	Nominal composition of this 16-5 steel is	25
4	Test Parameters for slurry erosion testing	26
5	Mechanical properties of as received sample	29



## ABSTRACT

The silt erosion resistance of non-nitrided and nitrided 16-5 martensitic stainless steel AISI 431 was evaluated according to ASTM G32 standard. Nitriding was carried out in BHEL Haridwar with a mixture of ammonia gas for the duration of 25hrs. The microstructure of the AISI 431 steel was characterized by optical and scanning electron microscopy, along with by X-ray diffraction. Expanded martensite and iron nitrides were produced at the surface of the 16-5 martensitic stainless steel. XRD analysis along with curves of weight loss, comparison between two steels and roughness parameters of both steels were also plotted as a function of exposure time of 16 Hrs. The 28.6+5  $\mu\text{m}$  thick nitride layer has been formed and it showed two distinct regions: a first 5  $\mu\text{m}$  thick of white layer and just underneath the surface comprising precipitated  $\epsilon$   $\text{Fe}_3\text{N}$  and  $\gamma$   $\text{Fe}_4\text{N}$  nitrides and expanded  $\alpha$  martensite and then rest is simply martensite. Iron nitride precipitation significantly reduced the incubation period, letting detachment of entire grains due to the impact of shock-waves over the surface. Regardless of this, after elimination of the first 5  $\mu\text{m}$  thick layer, the silt erosion resistance enhanced considerably. The correlation between weight loss and time-variation curves, wear mechanisms and surface roughness along with micro hardness were also conferred.





# **CHAPTER – 1**

# **INTRODUCTION**

# 1. INTRODUCTION

Hydro Turbine segments, let's say, guide vane, runner blade, labyrinth, pivot ring, pump compressor, and so forth are known to be influenced by cavitation or blend of cavitation, silt erosion, and corrosion, as represented in Fig.1. Cavitation led erosion/pitting may surpass 40-mm depth beyond which a Hydroturbine runner is viewed as disastrous for operation and is for the most part taken out for the maintenance [1]. The cavitation penetration rate of basic parts, for example, impellor, turbine blades, and casing. A large amount of metal loss plainly demonstrates cavitation erosion as a serious issue One of the significant reasons for this is the presence of huge amount of quartz (90% or 5000-20,000 ppm) in the silt ( $\text{SiO}_2$ ,  $\text{Al}_2\text{O}_3$ ,  $\text{Fe}_2\text{O}_3$ ,  $\text{MgO}$ ,  $\text{CaO}$ , and so forth.), especially amid rainstorm season. Quartz which is known to have a high hardness Erosive wear of the turbine blades is a complex phenomenon that relies upon eroding particles, their size, shape, hardness and concentration, substrates chemistry, elastic properties, surface hardness and surface morphology and Operating conditions, speed and impingement angle  $\theta$ .

It ought to be stressed that silt erosion even with grain estimate under 60  $\mu\text{m}$  has prompted serious damage on pelton turbine 13Cr-4Ni and 16Cr-5Ni steels. These are utilized because of their amazing mechanical properties. Be that as it may, these materials are extensively less resistant to erosive wear and get damaged because of excessive amount of silt present in water. AISI 431 Martensitic stainless steel for assembling various mechanical parts of hydroelectric plants, for example, turbines, injectors and valves because of their great behavior in erosion and corrosion conditions, great weldability, high impact energy and high fracture toughness, among other valuable attributes. Despite their good properties, these steel experience surface damage due to the severe wear conditions found in hydropower plants.



*Fig. (1) Runner blades showing cavitation erosive failure [1]*

## 1.1 WHY MARTENSITIC STAINLESS STEEL?

Cavitation and silt erosion are intricate phenomena that occur in hydro turbines. Explosion of cavities roots a severe erosion to the base material due to high pressure wave created. AISI 431 Martensitic stainless steels (such as 16Cr-5Ni, 13Cr-4Ni) are, by far, the most popular choices for fabrication of turbine components, where cavitation erosion is the chief concern. For instance, runner blades are fabricated from various MSS such as 13Cr-1Ni, 13Cr-4Ni, 16Cr-5Ni, and 18Cr-8Ni stainless steel.

Low carbon i.e. less than 0.02% stainless steel called super martensitic stainless steel because it exhibits an exceptional combination of weldability, strength, toughness and corrosion resistance properties where as high carbon content martensitic stainless steels, e.g. AISI 440, will undergoes high hardness as well as high strength which will lead to exceptional wear resistance. Nevertheless, it has lower machinability index in comparison to low carbon martensitic stainless steel AISI 431. Hence, it would be better to take the low carbon martensitic stainless steels as an option and then coat it with suitable coating accordingly. After this machinability index will be improved, and consequently we obtain the better surface finish, and definitely a good wear resistance in comparison with the high carbon martensitic stainless steels.

Low carbon MSS has been progressively applied to critical structures and critical components such as water turbines, ship propellers, aircraft parts shown in fig (2). As well as oil country tubular imports – seamless pipes for drilling, casing and tubing for the application in oil and gas fields with further corrosive environments due to its excellent combined properties, which are actually dependent upon its chemical compositions and its special microstructures of SMSS. The chemical compositions of AISI 431 are grounded on Fe–Cr–Ni system with 4 to 6% of Ni, 0.5 to 2.5% of Mo, very low C of order ( $\leq 0.02\%$ ) and also varying micro alloying and nitrogen content which depends upon desirable properties. Martensitic lath microstructure can be attained even by air cooling (Normalizing) SMSSs from solution treatment temperature at austenite field because of their satisfactory hardenability.



*Fig (2) Turbine blade profile*

Successive tempering of SMSSs directly above  $AC_1$  temperature consequences in inverse transformation of martensite to austenite, which is comparatively stable and can be partly retained at room temperature. The retained austenite in martensite has been stated to be very effective to confer the ductility and toughness of SMSSs. Ever since we know Cr and Mo are the ferrite stabilizing components ( $\alpha$  phase), in martensitic stainless steels, it is essential to make austenite producing elements in order to avoid the occurrence of delta ferrite so that austenite phase is stabilized and martensitic transformation can take place upon air cooling. Nickel is the most common alloying element used to stabilize the austenite ( $\gamma$  phase) or expand the gamma phase field.

## 1.2 WHY COATINGS?

Numerous surface modification techniques has been employed satisfactory to enhance the tribological properties and good wear resistance of AISI 431 martensitic stainless steels. Among all these techniques, low temperature gas nitriding is an effective technique which has proven not only to improve the surface properties of stainless steels but also increase the life of turbine runner and impellor. High-quality cermet coatings were also employed in a similar way to improve properties of AISI 431. Usually HVOF coatings consist of tungsten carbide and chromium and cobalt act as binder (WC-Co-Cr). Turbine undergoing HVOF coating shown in fig (3). Nitriding is in practice for surface hardening of metallic components to improve their service life. The introduction of nitrogen atoms to steel substrate using thermochemical treatments has been proved to be an active technique to boost the wear resistance of stainless steels. N is also a very active austenite stabilizer.

In recent times, various austenitic and duplex stainless steels, nitrogen introduction to steel has been proved a good substitution over Nickel, because it not only reduce the cost but also offers customer an excellent combination of mechanical properties and corrosion resistance properties for MSS. The main benefits of nitriding over orthodox case hardening processes are, reduced cycle time and controlled development of the surface layer, elimination of white layer, reduced distortion of the component, no need of finishing (grinding, machining etc.), pore free surfaces are obtained. The extent of cavitation and silt erosion damage differs with the place of power stations and seasons. The silt erosion damage mechanism of all these coatings has been compared with the data available in the literature. The magnitude of hardness of silica particles used for this purpose was order of 800 VHN. It was decided that the blend of hardness and toughness in the nitriding coating led to the superior performance of steel in contradiction of both erosion and abrasion.

Development and use of more resistant materials, application of coatings, modification of components design, and minimizing silt contents in the water have been attempted to reduce the erosion. The micro-injection of bubbles (of non-condensable gases) to cover the component surface has also been tried to combat the erosion. Among these, Coatings/surface engineering appears most viable option to enhance the lifetime of the component. The physical and chemical processes involved with the cavitation erosion and response of materials have been presented. A study related to the declined performance of Hydroturbine components due to cavitation erosion have been described. This thesis tells about various coatings and coating methodologies developed to increase the erosion resistance and brief discussion on various aspects of erosion, metallurgical properties related to cavitation, and methods to characterize cavitation erosion have also been presented.



*Fig (3) Turbine undergoing HVOF coating*

### 1.3 Aspects of Silt Erosion

Hydraulic devices functioning in the range of high Reynolds's number amid  $10^6$  and  $10^{10}$  in the sediment carrying fluid experience erosion. In the case of Francis turbines, enlightens that the erosion occurs in the guide vanes due to the secondary flows from the spiral casing causing non-uniform flow angles at the inlet with high absolute velocities. The guide vane system is highly affected by the silt erosion. Wear mechanisms and its relationship with the particle material, angle of impingement, impact velocity and particle size. For ductile material, they have found that the maximum erosion occurs at impingement angle of  $30^\circ$ , whereas in brittle material, it occurs at  $80^\circ$  to  $90^\circ$  degree shown in fig (4).

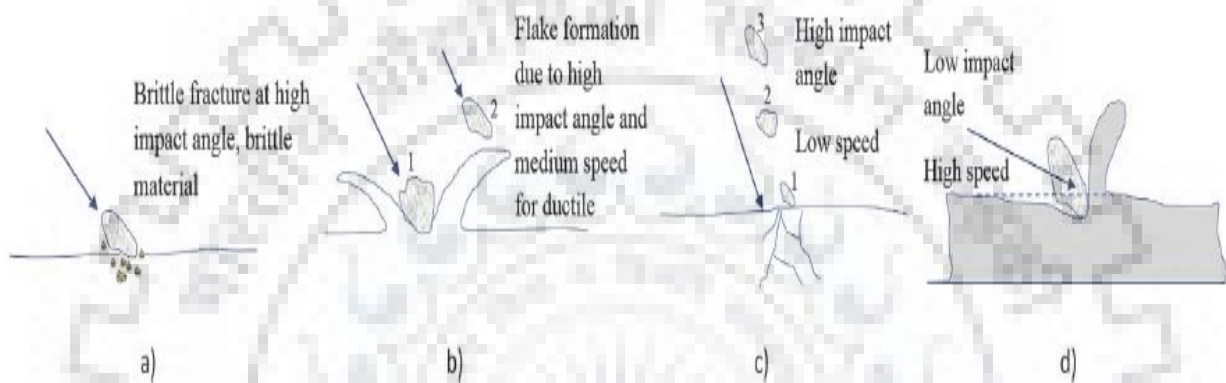


Fig (4 )Various forms of Erosive wear mechanisms a) Brittle fracture b) Plastic deformation c) Fatigue erosion d) Abrasive/cutting erosion [2]

### 1.4 Aspects of Cavitation Erosion

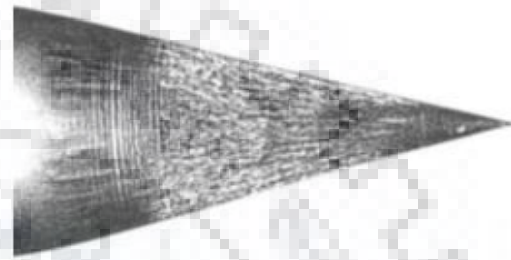
Cavitation erosion of equipment is notable result of cavitation together with the cavitation directed vibrations and noise, which diminishes the efficiency of power plants. Cavitation is a physical phenomenon which signifies the creation, growth, and collapse of bubbles [3]. It normally happens in conditions where high-velocity fluid flow encounters a pressure transformation. High fluid velocity in throttling range decreases the local pressure below the overall fluid vapor pressure causing in the formation of vapor bubbles

The mechanism of cavitation erosion is however not yet noticeably understood; the current understanding follows two explanations of cavitation erosion [4].When a bubble collapses within the liquid volume (symmetrical collapse), a shock wave originates into the adjacent fluid. When bubble in contact with or very adjacent to the solid boundary collapses in asymmetrical way. Here, the cavity is agitated from the side, away from the solid periphery, and lastly the fluid penetrates through the cavity in the form of micro-jet.

These mechanisms also lack explanation as shock waves are attenuated rapidly, and the radius of the cavity (micro-jet) is too insignificant to cause the cavitation erosion [5, 6]. The collapse of the cavity cloud might somewhat have more severe effect on the neighboring surface/solid boundary. Damage in Pelton turbine needle due to pure sand and combined effect of sand and cavitation erosion shown in fig (5) the procedure of frequent collapsing of bubble cloud can prompt a pressure intensity of as high as 1000 MPa, which is enough to bring about plastic deformation and resulting removal of metals/alloys. Plastic deformation, as a result of cavitation, is often proven by the waves/deformation bands and pile ups in the underlying material.



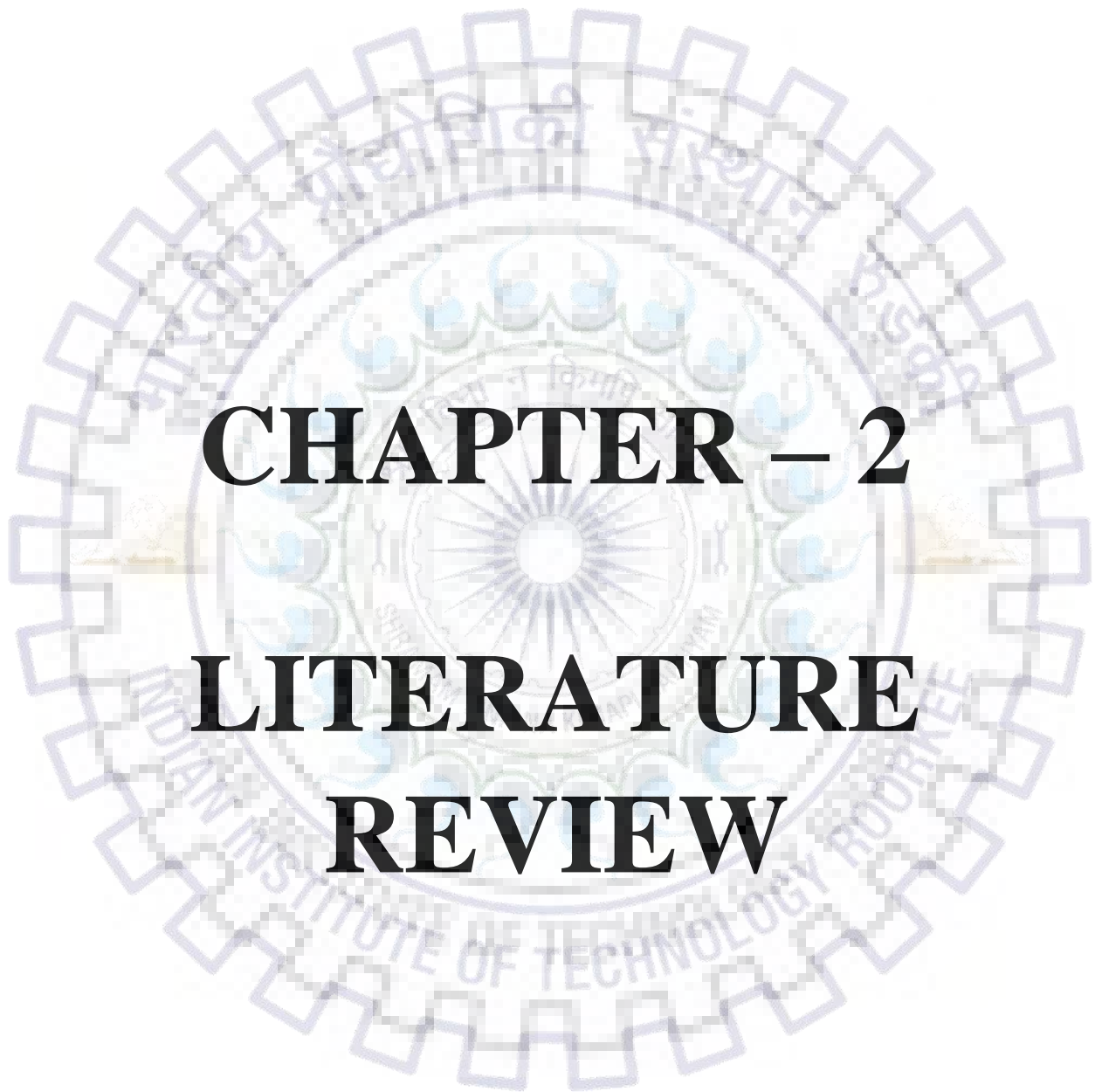
Pure sand erosion (wavy pattern)



Combination of cavitation and sand erosion

*Fig (5) Damage in Pelton turbine needle due to pure sand and combined effect of sand and cavitation erosion [3]*





# **CHAPTER – 2**

# **LITERATURE**

# **REVIEW**



## **2. LITERATURE REVIEW**

### **2.1 TURBINE MATERIALS AND SURFACE MODIFICATIONS**

Turbine blades in a water turbine are constantly exposed to fluid containing silt which contains high amount of quartz so, blades has to have high corrosion resistance properties and also have high strength to overcome erosion phenomena. The most commonly used material in hydro turbines are martensitic steel alloys that have 13% to 16% chromium to increase stability of the coating which improves corrosion resistance properties. The chromium content of these steel alloys exceeds the minimum amount of 12% then required to exhibit some atmospheric corrosion resistance. Having a higher chromium percentage in the martensite steel alloys allows for a much longer lifespan of the turbine blades. Greater weldability as well as better machinability is a necessary property that allows easy overhaul of the turbine blades. The different alloys used are MSS (16Cr-5Ni), MSS (13Cr-4Ni), and MSS (13Cr-1Ni)

### **2.2 Approaches generally been considered:**

1. Optimization of hydraulic design of the components i.e. turbine blades.
2. Development of a new cavitation-erosion-resistant alloys and coatings of various components.
3. Minimizing of silt contents in the water also been attempted to reduce the cavitation erosion.

Coatings/surface engineering appears to be most viable option to enhance the life of the component.

### **2.3 Various kinds of surface treatment processes**

#### **2.3.1 LASER HARDENING**

Thermal hardening of metals and alloys by laser radiation is based on local heating of a surface under the stimulus of radiation and successive fast cooling of this surface. Laser hardening of steels by similarity to other kinds of thermal hardening consists in formation of an austenite structure at a stage of heating and its successive transformation in martensite in a stage of cooling. The martensite needles were refined in laser-hardened steels due to the high-cooling rates. The hardness distribution along the cross section of the laser-hardened steels were shown in fig (6). The hardness was higher in melted region in laser-hardened steels because of the formation of Martensite due to very high cooling rates.

#### **2.3.2 NITRIDING**

Plasma nitriding is a modern and environmentally clean method of nitriding it permits a fully automated and controlled nitrogen-diffusion process, which makes it possible to nitride the steel surfaces without compound or white layer formation. Therefore plasma nitriding reduces finishing costs and more importantly it reduces the tendency of spalling the microstructure of the pulsed-plasma nitrided steels. The nitrided layers consist of FeN, Fe<sub>2</sub>N, Fe<sub>3</sub>N, Fe<sub>2</sub>N<sub>3</sub> and Fe<sub>3</sub>N<sub>4</sub> phases in diffused layers. The nitriding layers range from tens to hundreds of microns and these are perfect for improving wear resistance

The advantages of plasma nitriding over conventional nitriding processes are, reduced cycle time, and controlled growth of the surface layer, elimination of compound layer, reduced distortion of part, no need of processing (grinding, machining etc.), and pore free surfaces without major defects present.

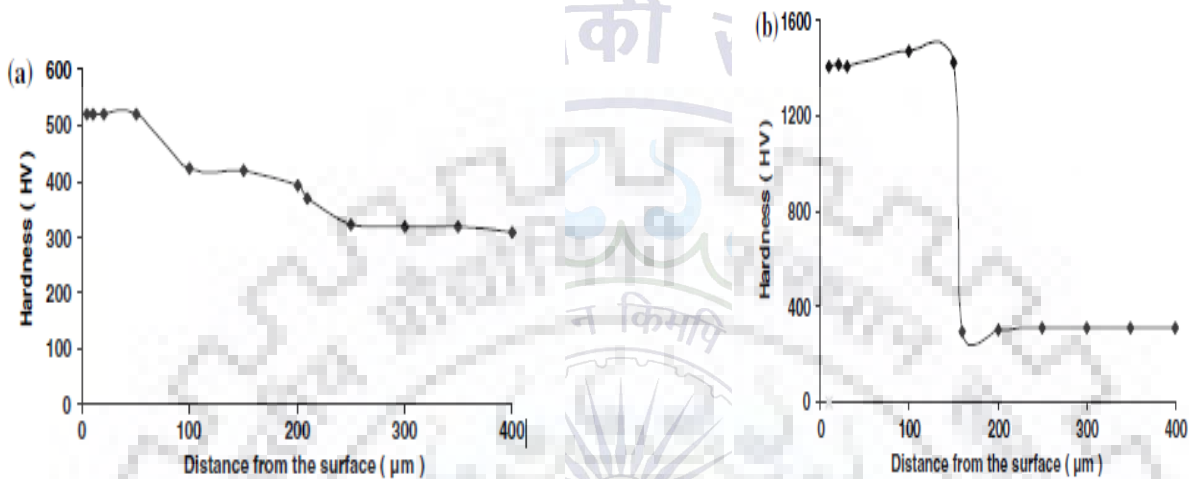


Fig (6) Cross-sectional hardness distribution of (a) laser-hardened 13Cr-4Ni steels (b) pulsed-plasma nitrided 13Cr-4Ni steels [11]

### 2.3.3 High-velocity oxy fuel (HVOF) spraying

HVOF spraying has been considered an asset to the family of thermal spray processes exclusively for materials with melting point less than 3000 K. It has proven successful, since it shows more advantages in density and bond strength making so, it is attractive among many wear and corrosion resistance applications [8-9]. Its high coating quality results from the use of a hot combustion-driven high-speed gas jet for thermal spraying. Shown in fig (7) these coatings have environmental advantages compared to chemically/electrochemically formed coatings. Tungsten carbide powders are widely used in the HVOF spraying system [10]. These are used to yield dense, high hardness and excellent wear resistance coatings commonly to combat the erosion and corrosion taking place in hydropower plants and pumps.



Fig (7) The HVOF coating process being adopted on a spear of a Pelton turbine [12]

## 2.4 Effect of Angle of Impingement

Erosion of a material is also depends upon the angle at which the erodent particles i.e. quartz strikes at the surface. It has been found that maximum erosion rate for a ductile material is at impingement angle of approximately 20 to 30 degree and, it decreases as angles goes on higher side. This phenomena contrasts with brittle materials where the loss of material due to erosion rises steadily with angle, reaching a peak at 90 degree. Hence, coatings, which displays good performance, close to or at near normal incidence angles may not exhibit the same performance at low-incidence angles. Thus, the effect of angle of impingement has comes as an important parameter, since the silt entrained in water impinges at various incidence angles over the surface of the components in actual turbine atmosphere. Figure (8) shows the amount of erosion in terms of mass loss after 1 h of testing at various angles of impingement. It can be observed that the laser-hardened 13Cr-4Ni steel exhibited better results than the pulse plasma nitrided 13Cr-4Ni steels particularly, at low angles of impinge

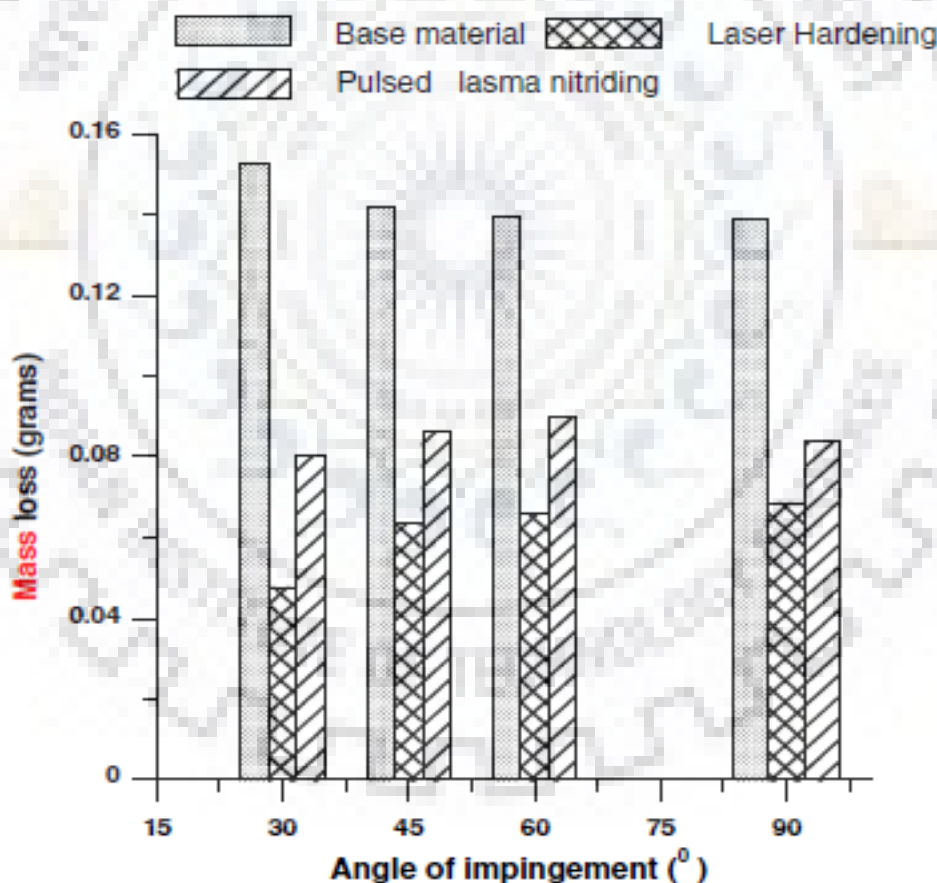


Fig (8) Erosion loss for modified steels and as received material at various angles of impingement [11]

Materials/coatings	Micro hardness (HV)
WC 636 HVOF coating	1090–1226
Nitrided 13Cr–4Ni steel	774–942
Nitrided 12Cr steel	1000–1200
12Cr steel	290–300

Table 1 micro hardness of different coatings [9]

### 2.4.1 Comparison between plasma nitriding and HVOF coatings

The performance trends for all these coatings are similar to the abrasion test results obtained using ASTM G-65. For all the coated as well as uncoated steels, a drastic reduction in volume loss is observed Under identical erosive and abrasive wear test conditions, The HVOF coated steel performed much better than plasma nitrided 12Cr and 13Cr–4Ni steels. The microstructures of HVOF sprayed tungsten carbide show a few voids as defects. The microstructures of plasma nitrided 12Cr and 13Cr–4Ni steels are free from all these defects. However, they lack the resistance to abrasive and erosive wear as their micro hardness values are below those of the erodent (<1100). Plasma nitrided 12Cr steel performed much better than plasma nitrided 13Cr–4Ni steels. This is due to its higher micro hardness and its ability to absorb more nitrogen under identical plasma nitriding experimental conditions. Shown in fig (9) the superior performance of HVOF coating is due to the hardness of tungsten carbide particles (1800 HV). These are well embedded in the matrix and their percentage is much more than iron nitride phases in the 12Cr plasma nitrided steel.

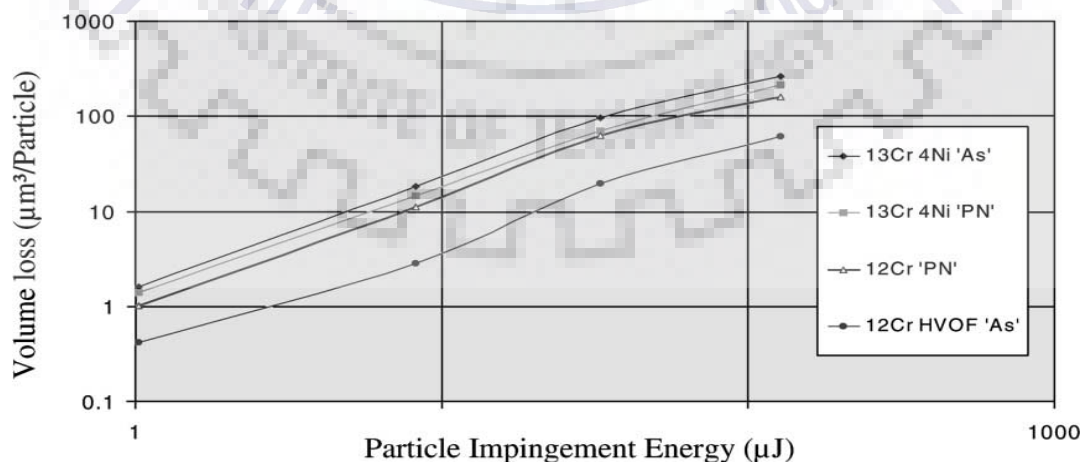


Fig (9) Relationship between erosion rate and particle impingement energy. [11]

## 2.5 Plasma Nitrocarburising

Plasma ion-nitrocarburising is also a method of surface hardness of steels which will increase hardness by diffusion of Carbon and nitrogen atoms up to a few hundred micron depth (case) under the surface. It takes place in the ferritic region without advent of any phase transformation. The solubility of carbon and nitrogen in the ferrite region is very small and most of the carbon and nitrogen that enters to steel will forms hard nitrides and carbides. In usual gas nitrocarburising technique, the outer layer formed is called the “white Layer” which is very hard as well as brittle. This layer has to be removed by grinding because it is undesirable. However, in plasma ion-nitrocarburising this white layer can be avoided by a adequate choice of plasma parameters including temperature limits, and LPG, NH<sub>3</sub> gases flow rates as well as the applied and bias voltage. [12]

Fine hard steel shots of size 200  $\mu\text{m}$  at a pressure of 3.5 kg/cm<sup>2</sup> before they were plasma nitro carburized and studied for their cavitation behavior. It is well known that dislocation densities and grain size are important factors that enhance the nitrogen diffusion process in steels [13-17]. Surface texturing increases the dislocation density and refines grain size of the base material. Volume loss data have been calculated from the weight loss for both samples shown in fig (10). Generally 13cr-4ni steel sample has density ( $\rho = 7.85$  g/cc), and Hvof sample ( $\rho = 12.7$  g/cc).

The Vickers micro-macro-hardness tester was used to carry out micro-hardness as well as case depth measurements of the samples. Vickers hardness as a function of depth below surface as shown in fig (11). The advantages of the Vickers hardness test are that extremely accurate readings can be taken and just one type of indenter is used for all types of metals.

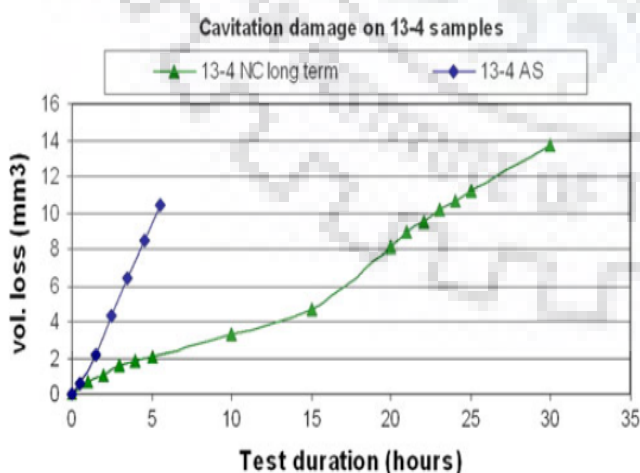


Fig (10) Volume loss by cavitation erosion after removal of nitro carburized

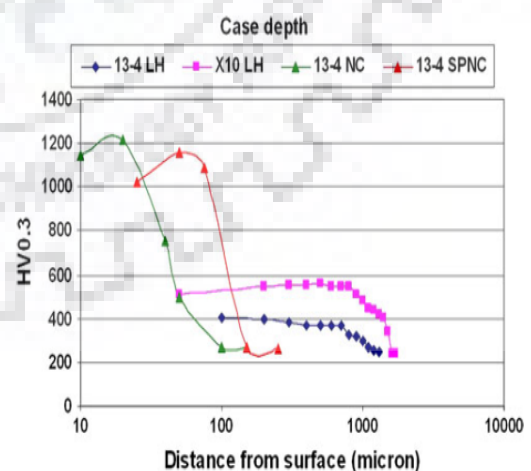


Fig (11) Vickers hardness as a function of depth below surface

## Volume loss due to cavitation as a function of test duration

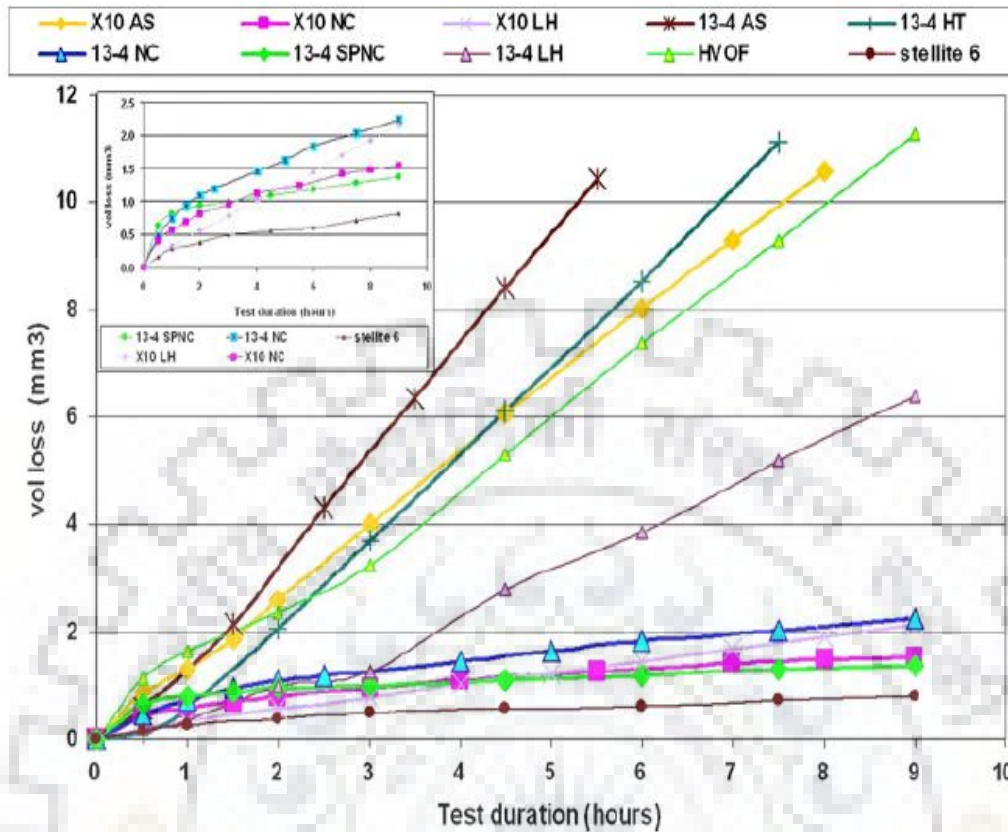


Fig. (12) Volume loss due to cavitation as a function of test duration [12]

Sl. no.	Sample ID	Sample composition and treatment	Comparison after 5.5 h of cavitation testing
1.	13-4 (AS)	13Cr-4Ni as-received steel sample	Untreated
2.	13-4 (HT)	13Cr-4Ni as-received steel heat-treated sample	1.4-fold better than 13-4 (AS)
3.	13-4 (LH)	13Cr-4Ni laser treated at 1550 °C at 2 mm/s	2.9-fold better than 13-4 (AS)
4.	13-4 (SPNC)	13Cr-4Ni shot peened and nitrocarburized steel sample	9 fold better than 13-4 (AS) and 5.8-fold better than HVOF
5.	13-4 (NC)	13Cr-4Ni nitrocarburized steel sample	6-fold than 13-4 (AS)
6.	X10 (AS)	X10CrNiMoV1222 as-received sample	Untreated
7.	X10 (LH)	X10CrNiMoV1222 laser treated at 1550 °C at 2 mm/s	5.6-fold better than X10 (AS)
8.	X10 (NC)	X10CrNiMoV1222 nitrocarburized steel sample	6-fold better than X10 (AS) and 5.5-fold better than HVOF
9.	HVOF	HVOF-coated WC-Co-Cr coating	...
10.	Stellite 6	Stellite 6 laser clad sample	Benchmark for cavitation

The cavitation erosion is measured by the **mean depth of erosion rate** (MDER) which gives the relative performance of the samples and is calculated by the following equation

$$\text{MDER } (\mu\text{m/h}) = 1000\Delta V / (A \times \Delta t)$$

Where  $\Delta V$  is the volume loss in  $\text{mm}^3$ ,  $\Delta t$  is the duration of the test in hour,  $A$  is the surface area of the specimen in  $\text{mm}^2$ .

## 2.6 Characteristics of a protective coating are:-

1. Cavitation resistance,
2. Abrasion resistance,
3. Strong bonding to the substrate,
4. Corrosion resistance,
5. Vibration damping,
6. Easy applicability at the site.
7. To improve wear resistance properties of turbine material
8. To achieve good Tribological properties
9. Life of runner should be improved

## 2.7 Gas nitriding

The introduction of nitrogen atoms by the help of thermochemical treatments that has been proved to be an effective way to improve the wear resistance of stainless steels. Nitriding processes is based upon solid, liquid as well as gas treatment. Plasma nitriding is a glow discharge process in which a mixture of nitrogen and hydrogen gases usually plasma is used which improves the resistances against fatigue, wear, and corrosion. The ammonia may also be diluted with nitrogen or hydrogen. Shown in fig (13) .The parts which is to be nitrided are loaded on fixtures or also in the “baskets”. Purging of the furnace with nitrogen must be done before ammonia can be let into the furnace so that risk of explosion must be discarded.

PROCESS	NITRIDING	PLASMA NITRIDING
Medium	NH <sub>3</sub> /N <sub>2</sub> /H <sub>2</sub> gas	Nitrogen plasma
Temp:	500–550 °C	450–580 °C
Time:	5–25 h	10 min – 30 h

Table 2 Process parameters of plasma nitriding and gas nitriding

The principal phases that form while nitriding of iron as the base materials (steels) are first a solid solution of alpha-iron ( $\alpha$ ), which has a maximum solid solubility of about 0.11 wt. % nitrogen. The next phase that will form is gamma-prime ( $\gamma'$ ). This phase field has a solubility range of about 5.1 to 6.1 wt. % nitrogen, depending on temperature limits, and is normally represented by the chemical formula  $\text{Fe}_4\text{N}$ . The third phase is epsilon ( $\epsilon$ )  $\text{Fe}_{3-2}\text{N}$  and it may also have equilibrium nitrogen contents of 7 to 8 wt. % nitrogen, depending on the temperature at which it will form. A "white layer", that appears microscopically, on the surface of the nitrided specimen. This white layer is composed of  $\gamma$  and/or  $\epsilon$ . It may also contain  $\text{Fe}_2\text{N}$  and various iron-nitrides. Thermodynamically, cannot form below  $577^\circ\text{C}$  ( $1070^\circ\text{F}$ ).

These phases present in the white layer may have desirable and/or undesirable features depending on the proposed application. Consequently, it is important to be able to control the nitriding process is to produce the desired structure in terms of the composition of the white layer. Gas nitriding is generally accomplished by an atmosphere of ammonia ( $\text{NH}_3$ ) in a mixture of nitrogen ( $\text{N}_2$ ), or dissociated ammonia ( $\text{D-NH}_3$ ), or hydrogen ( $\text{H}_2$ ). All of the above gases are adsorbed on the surface of the steel and form a gas layer. Fresh ammonia must diffuse through this layer, or the layer can be swept away. This why it is beneficial to have a dynamic, rather than a static, atmosphere to sweep away the layer. The radicals  $\text{NH}_2$  and  $\text{NH}$  have a much higher adsorption potential than the  $\text{NH}_3$  molecule. Therefore, the step-by-step breakdown of the  $\text{NH}_3$  molecule accelerates the adsorption. The N and H atoms diffuse into the iron lattice, while the NH radicals diffuse along the grain boundaries. The hydrogen that goes into the metal is a reversible reaction, and diffuses out to form molecular hydrogen that is liberated.

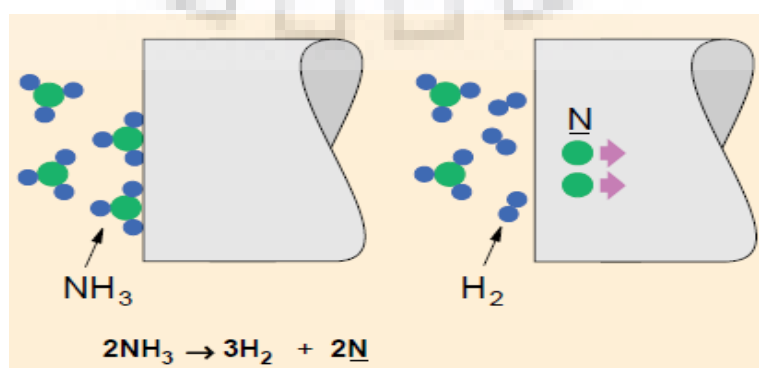


Fig (13) Schematic diagram showing Nitriding process



If the nitriding reaction is permitted to continue uncontrolled process then, nitrides ( $\gamma$  and/or  $\epsilon$ ) begin to form at the surface from the buildup of nitrogen shown in fig (14). If permitted, this nitride layer (compound layer) will become continuous, and at the second stage of nitriding begins; the nitrogen coming out from and through the white layer towards the base metal at a much slower rate. In summary:

Stage I: Nitrogen is absorbed into the alpha-ferrite.

Stage II: Solubility limit had been reached in ferrite and gamma-prime starts to form.

Stage III: Solubility limit of gamma-prime had been reached and epsilon starts to form.

As the reactions proceed further from Stage I to Stage III, the diffusion of nitrogen into the base metal becomes progressively slower. Therefore, it seems plausible that a process that avoids Stages II & III would develop the desired depth of the alpha solid solution more quickly

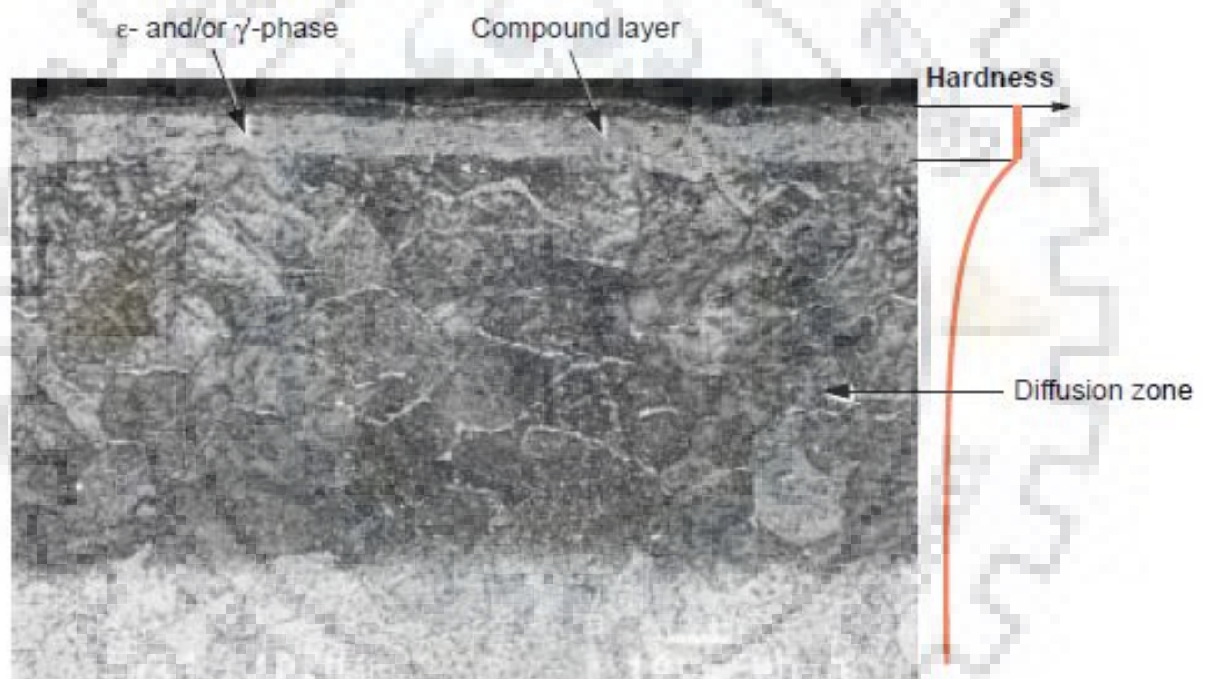
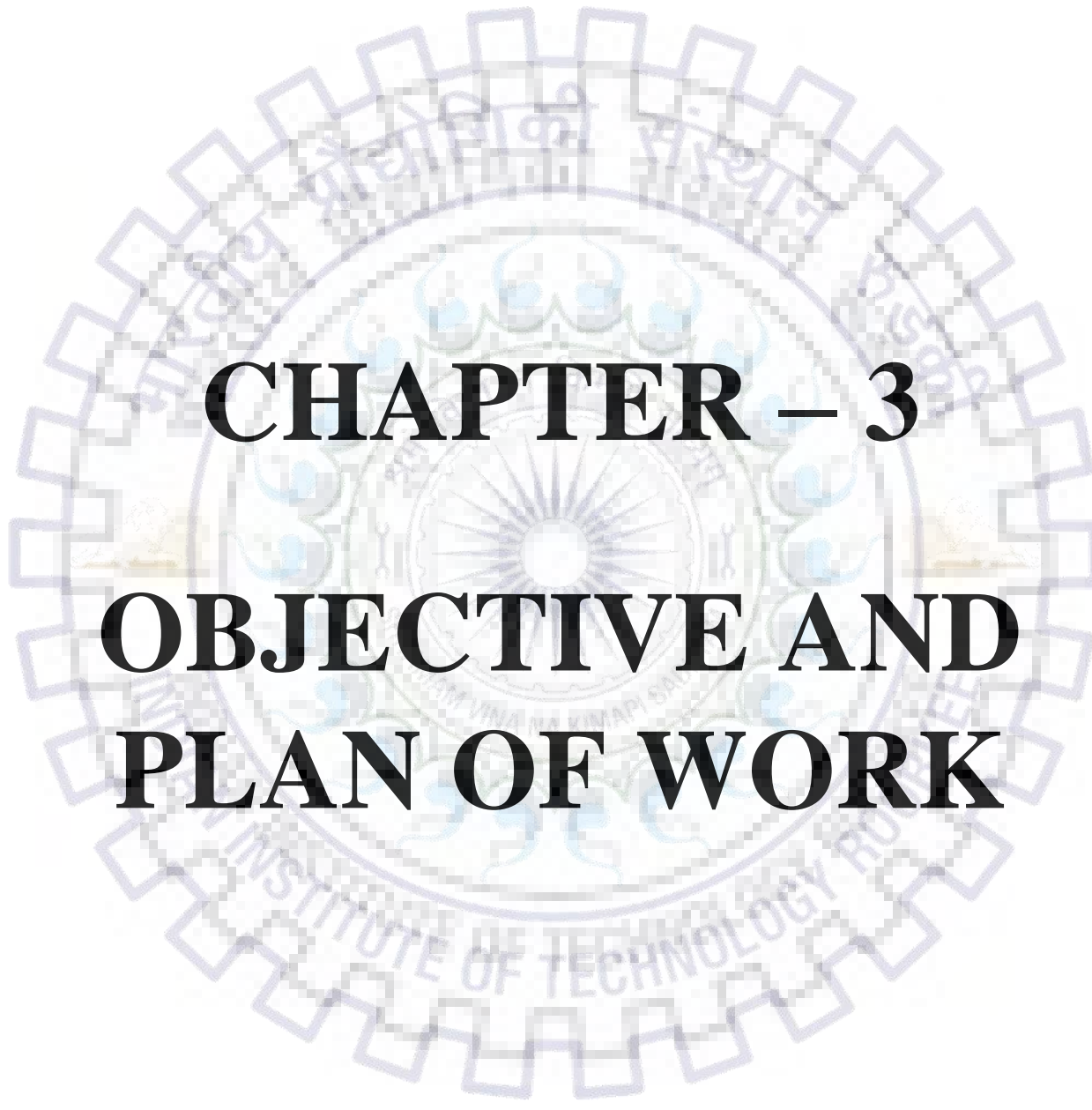


Fig (14) Micrograph shows both the compound layer and the underlying diffusion zone



# **CHAPTER – 3**

# **OBJECTIVE AND**

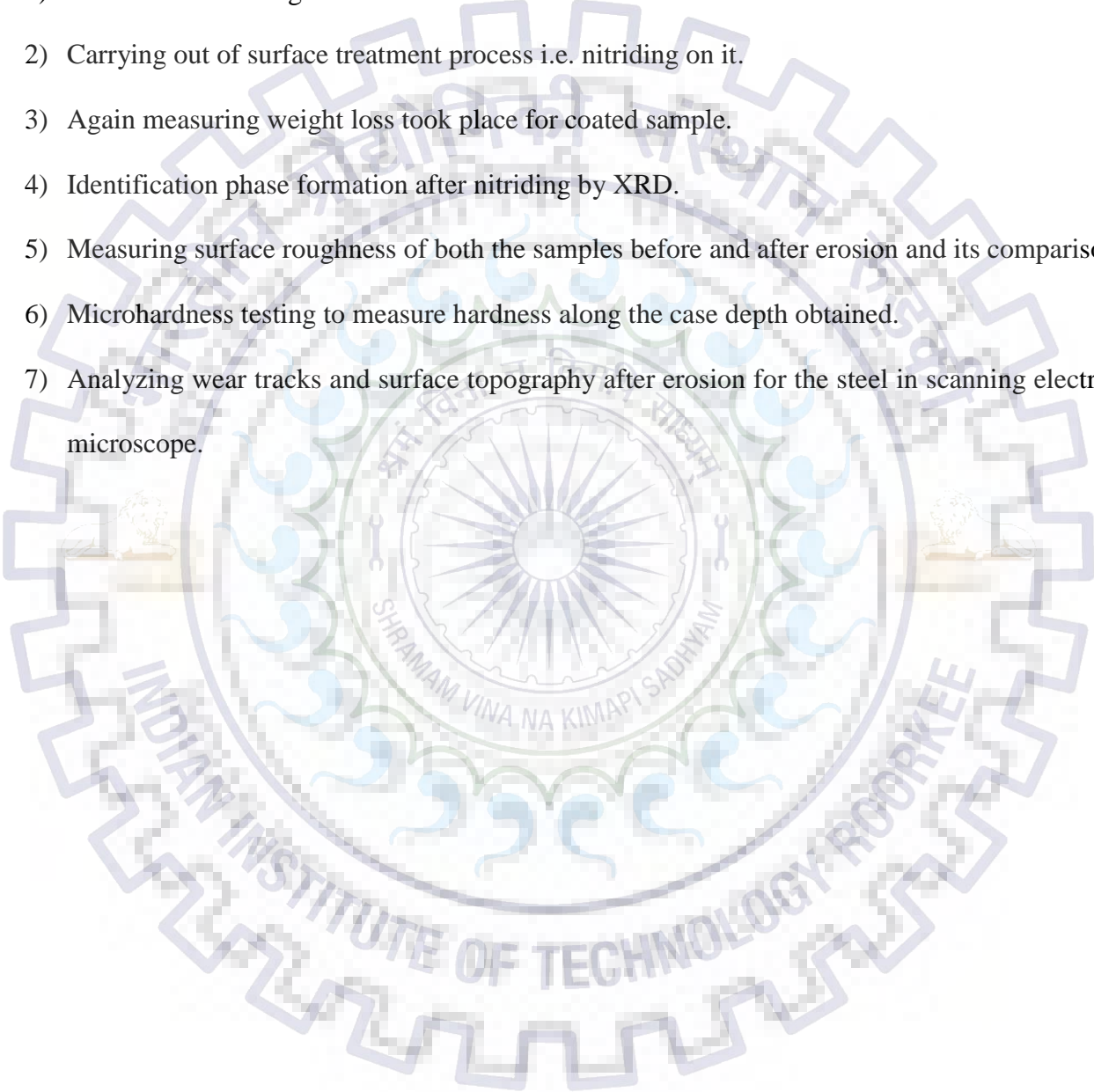
# **PLAN OF WORK**

### 3. OBJECTIVES AND PLAN OF WORK

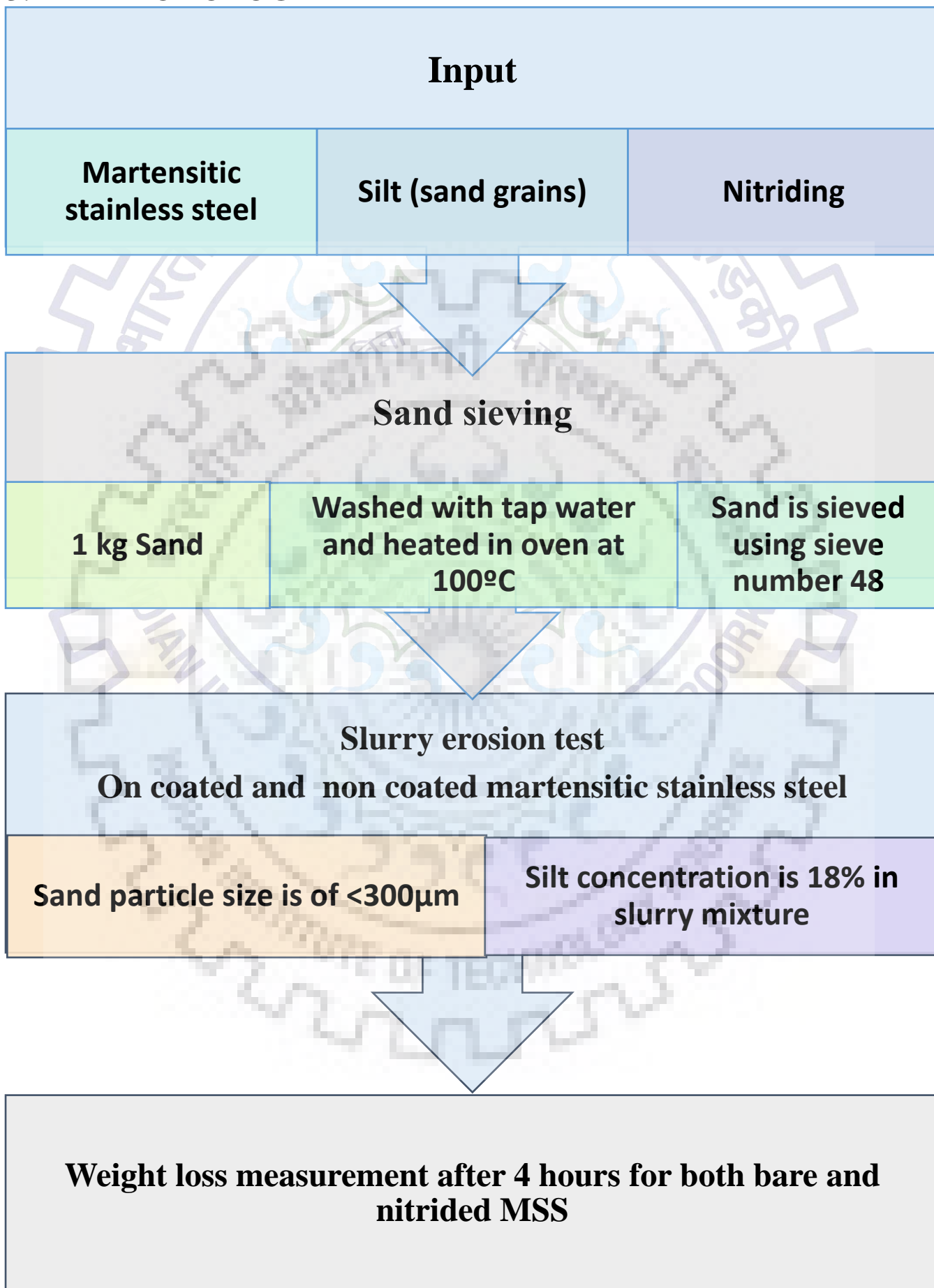
#### 3.1 OBJECTIVES OF WORK

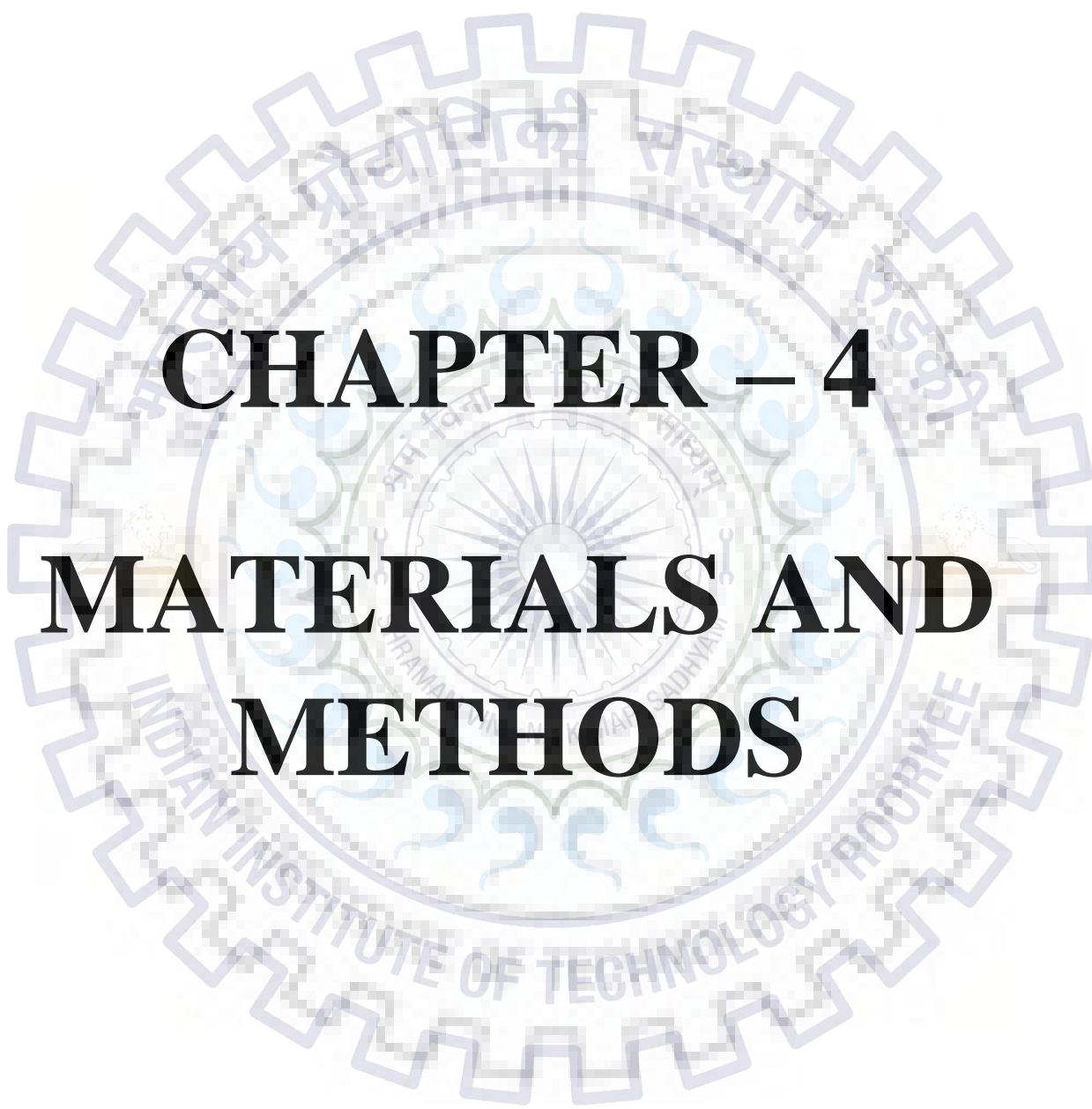
The aim of the present study is:

- 1) To measure the weight loss of non-coated martensitic steel
- 2) Carrying out of surface treatment process i.e. nitriding on it.
- 3) Again measuring weight loss took place for coated sample.
- 4) Identification phase formation after nitriding by XRD.
- 5) Measuring surface roughness of both the samples before and after erosion and its comparison.
- 6) Microhardness testing to measure hardness along the case depth obtained.
- 7) Analyzing wear tracks and surface topography after erosion for the steel in scanning electron microscope.



## 3.2 METHODOLOGY





# **CHAPTER – 4**

# **MATERIALS AND**

# **METHODS**

## 4. MATERIALS AND METHODS

### 4.1 AISI 431 Martensitic stainless steel

*Nominal composition of this 16-5 steel is*

<b>C &lt;0.05</b>	<b>Avoids problem due to sensitization</b>
<b>Cr 15-16</b>	<b>Corrosion resistance property cr&gt;12% Ferrite stabilizer</b>
<b>Ni 4-5</b>	<b>Imparts ductility and toughness Austenite stabilizer</b>
<b>Si 0.1-0.35</b>	<b>Carbide formation is delayed</b>
<b>P 0.025</b>	<b>Increases hardenability</b>
<b>Cu 3-3.7</b>	<b>Imparts ductility</b>
<b>Nb 0.2-0.35</b>	<b>Strong carbide former</b>

Table 3 Nominal composition of this 16-5 steel

Analysis Report 10/30/17 11:56:55 AM Page

Method: STAINLES Sample Name: Preetika M.Tech. Operator:

Run Time: 10/30/17 11:53:39

Comment:

Mode: CONC Corr. Factor: 1

Elem	C	Si	Mn	P	S	Cr	Ni
Avg	.0054	.2405	.3992	<.0000	.0030	15.74	3.703
SDev	.0012	.0042	.0041	.0004	.0000	.11	.008
%RSD	21.33	1.744	1.019	65.85	1.347	.6948	.2178
#1	.0062	.2434	.3963	<.0000	.0030	15.82	3.697
#2	.0046	.2375	.4020	<.0000	.0029	15.66	3.709

Elem	B	Cu	Mo	Base Fe
Avg	.0018	1.983	.1338	77.792
SDev	.0001	.007	.0168	.1092
%RSD	2.628	.3303	12.53	.11871
#1	.0018	1.988	.1219	77.727
#2	.0018	1.978	.1456	77.857

IntStd	1	2	3	4	5	6	7
Mode	Counts	NOTUSED	NOTUSED	NOTUSED	NOTUSED	NOTUSED	NOTUSED
Elem	Fe	---	---	---	---	---	---
Wavlen	273.074	---	---	---	---	---	---
Avg	11620	---	---	---	---	---	---
SDev	290.6209	---	---	---	---	---	---
%RSD	2.501094	---	---	---	---	---	---
#1	11414	---	---	---	---	---	---
#2	11825	---	---	---	---	---	---

Fig (15) Spectroscopy results of as received

As received sample of martensite stainless steel size of ( 85 x12 x15 )mm

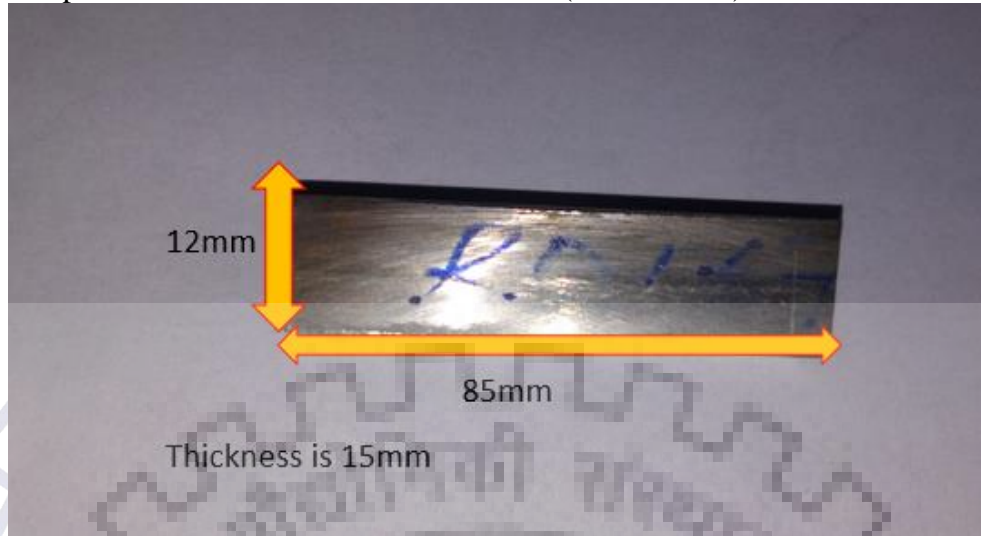


Fig (16) Dimensions of as received sample

Further 4 samples are cut from as received sample by wire cut EDM

To study of silt erosion in martensitic stainless steel sample is used of dimension (10 x 10 x 3 mm).

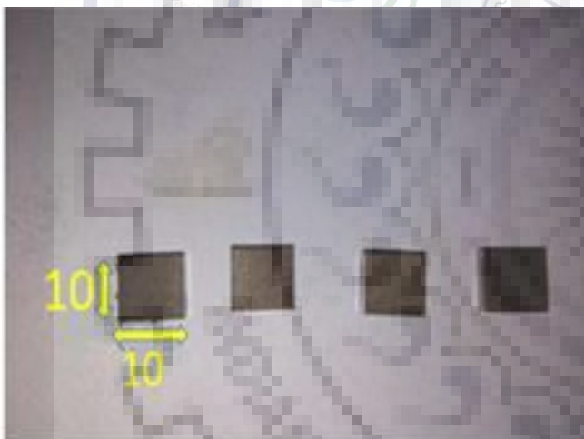


Fig (17) samples obtained after wire cut EDM

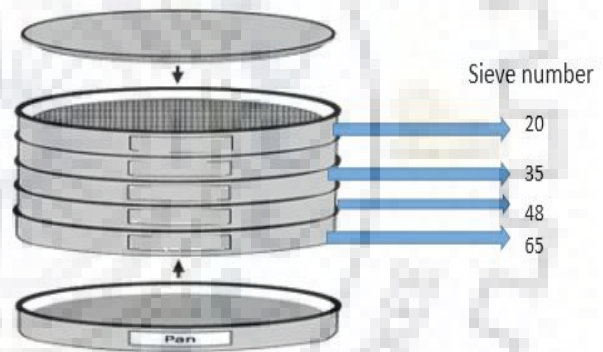


Fig (18) Sand sieving pans

### Test parameters

1. Silt particle concentration	18%
2. Total duration of test	16hrs
3. Cycle time	4hrs
4. Particle size used	300 $\mu$ m
5. Angle of impingement	0° 30° 60° 90°
6. Total silt used	10 kg
7. Temperature	Room temp
8. Sample mounting position	Static
9. Type of abrasive particles	Regular silica grains

## 4.2 Slurry erosion tests

The slurry erosion tests were carried out, in which the specimens were submitted to wear conditions similar to those of the liners of Francis hydraulic turbines. Fig.14 shows the configuration of the testing machine, which is composed of a sample holder connected to an electrical motor. Test is performed at room temperature. The samples were pasted at the sample holder at different angle of inclination to ensure grazing incidence of the particles (see Fig.13). The slurry was composed of normal tap water and quartz particles i.e. regular sand with a mean diameter is in between 212 and 300  $\mu\text{m}$  (AFS 50/70) and the solids content i.e. slurry concentration was 18 wt%. The erosion resistance was determined from the mass loss results. Mass losses were measured every 4hrs by using a scale with 0.01 mg resolution. The total duration of each test was 16 hrs, and after that period both the sample and the slurry were replaced



*Fig (19) sample holder of slurry testing machine*



*Fig (20) Slurry Erosion Testing Machine*



### 4.3 Microhardness test

It is a method of determining a material's hardness or resistance to penetration when test samples are very small or thin, or when small regions in a composite sample or plating are to be measured. It can provide precise and detailed information about surface features of materials. The hardness test is performed by applying controlled force of 1000 grams or less for a specific amount of time to an indenter in a rhombus-shape (elongated four-sided pyramid). The hardness of the material is determined by the depth to which the indenter penetrates. The impression is measured microscopically and, when combined with the amount of the test load, can be used to calculate the hardness value on the Knoop scale. Knoop hardness numbers are often cited in conjunction with specific load values.



*Fig (21) Microhardness Testing Machine*

During microhardness testing, a diamond indenter is pressed into the material's surface with a penetrator and a light load of up to 1000 grams. The result of applying the load with a penetrator is an indent or permanent deformation of the material surface caused by the shape of the indenter.

Both the Knoop and Vickers hardness test methods use specific measurements from the indent, in conjunction with formulas, to calculate material hardness. Accurate measurement of the resulting indentation requires the use of a special microhardness testing microscope because the indents are so small. The Knoop hardness test uses a narrow rhombus shaped diamond indenter. The test surface usually must be highly polished.

Forging shall be heat treated to get desired mechanical properties

Intermediate annealing >60 min at 1020 to 1050 degree

Solution annealing >60 min at 820 to 850 degree air cooling below 30 degree

Precipitate hardening 120 min at 530 to 560 degree

Duration of heat treatment as well as controlled cooling rate are to be chosen to achieve minimum residual stress.

### ***Mechanical properties of sample***

<b>0.2% Proof stress</b>	<b>930-1000N/mm<sup>2</sup></b>
<b>Tensile strength</b>	<b>&lt;1040 N/mm<sup>2</sup></b>
<b>% Elongation</b>	<b>13 min</b>
<b>% Reduction in area</b>	<b>50 min</b>
<b>Impact values</b>	<b>100 J/min</b>
<b>Brinell hardness HBW</b>	<b>295-335</b>

Slight deviation in chemical composition is permissible

We observed that

Percentage of nickel is found out to be less

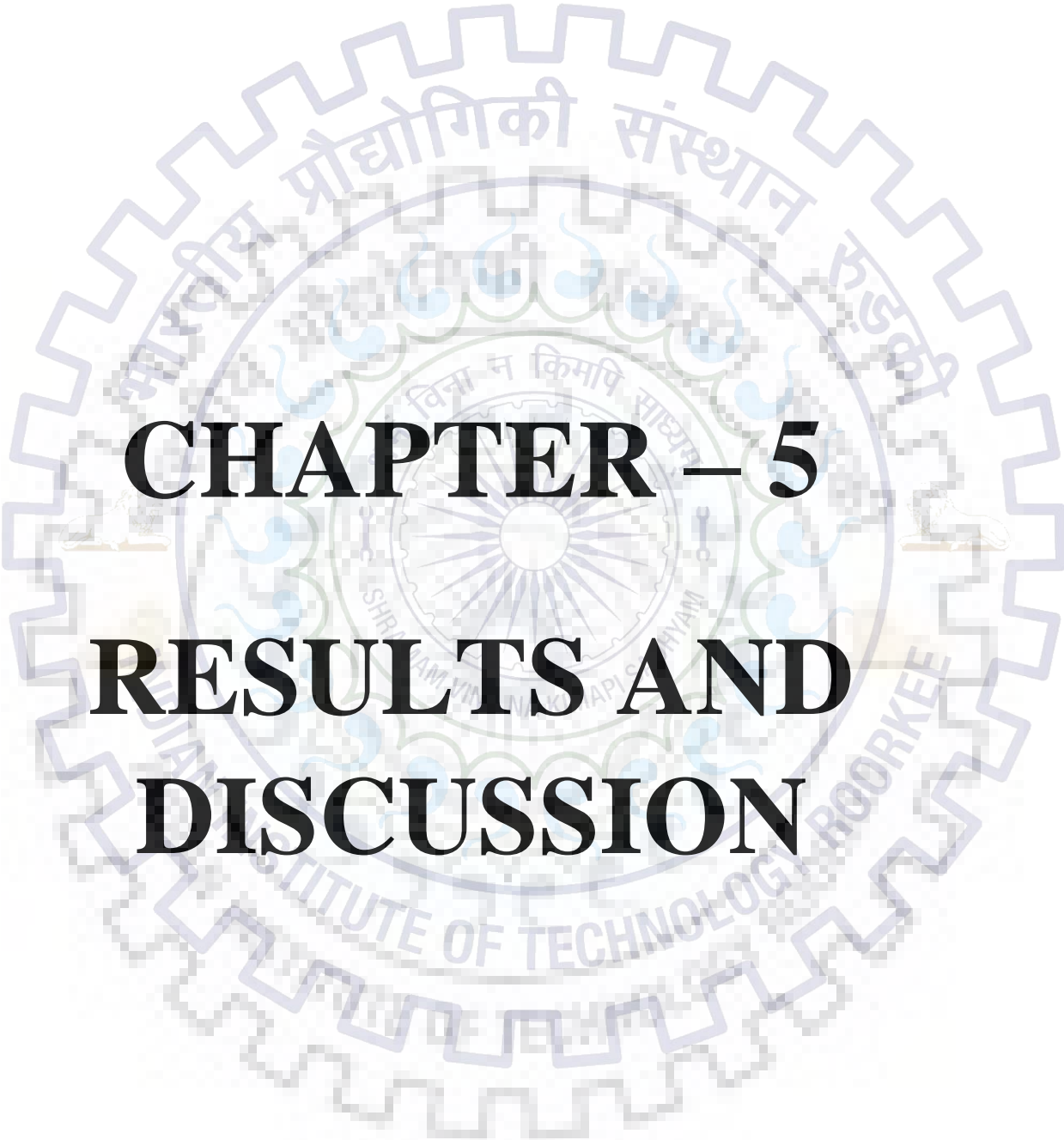
Amount of phosphorous is very less so we found some traces of it

We also found some traces of boron and molybdenum.

As steel contains alloys like copper and Niobium

Carbon percentage is <0.05 %

Rest is iron around 77 .8 %



**CHAPTER – 5**

**RESULTS AND**

**DISCUSSION**

## 5. RESULTS AND DISCUSSIONS

### 5.1 SEM Analysis of silt

- Silt used in experiment is a regular sand found abundant in nature.
- Largest particle size used in study were up to 300  $\mu\text{m}$ .
- Sand particle range from very fine to fine sand in size.
- Shape of particles ranges from semi round to sub angular.
- SEM image of abrasive particles before slurry erosion test.
- Change in size distribution shown in fig (22)
- Edges are sharp and pointed.
- Note that after the tests the distribution is shifted to smaller grain sizes.

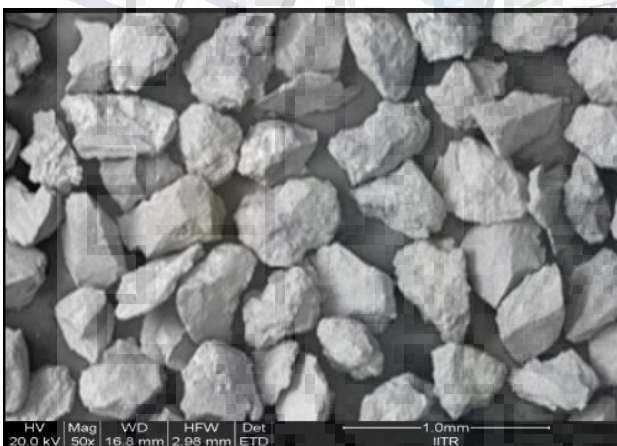


Fig (22 a) SEM image of abrasive particles before test

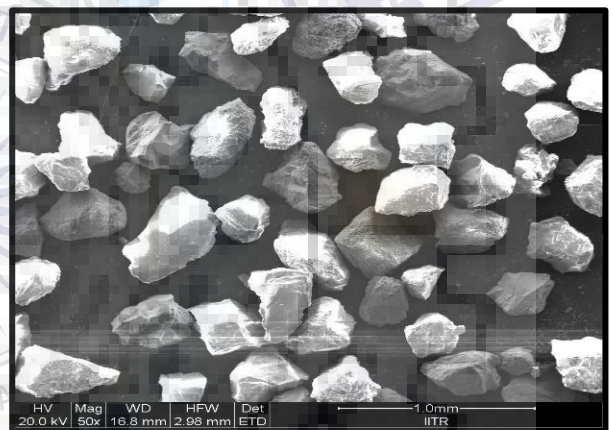


Fig (22 b) SEM image of abrasive particles after test

Morphology of abrasive particles Analysis depends on:-

- Eroding particles size, Shape Hardness, concentration of silt used.
- Substrate chemistry elastic properties surface hardness and surface morphology.
- Turbine operating condition velocity and impingement angle.

## 5.2 Microstructure analysis

- The microstructure composed of tempered martensite along with retained austenite and delta ferrite in it.
- The prior austenite grains were subdivided into packets of thin laths (needles) of martensite.
- Due to high chromium atom mobility, chromium carbide formation will be very prominent when the temperatures reaches above 425 °C
- Formation of chromium carbide leads to depletion of chromium in the adjacent areas.
- Although MSS has a very low carbon concentration, intergranular stress corrosion cracking (IGSCC) had been observed due to formation of Cr depleted zones due to precipitation of Cr carbide.

So corrosion resistance is highly reduced in neighbor regions. In this case after etching, the regions are seen dark which is an evidence of chromium carbides presence shown in fig (23)

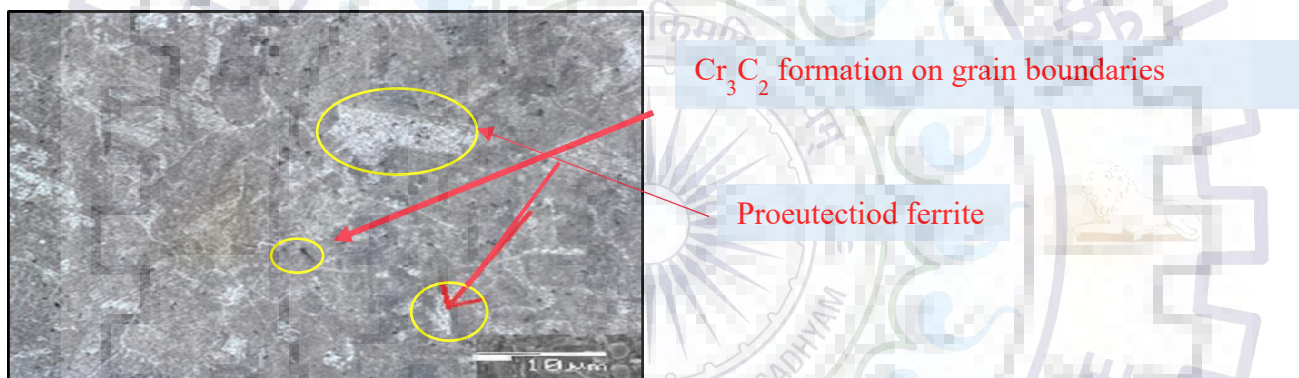


Fig (23a) optical image of 16- 5 MSS depicting pro-eutectoid ferrite and chromium carbide

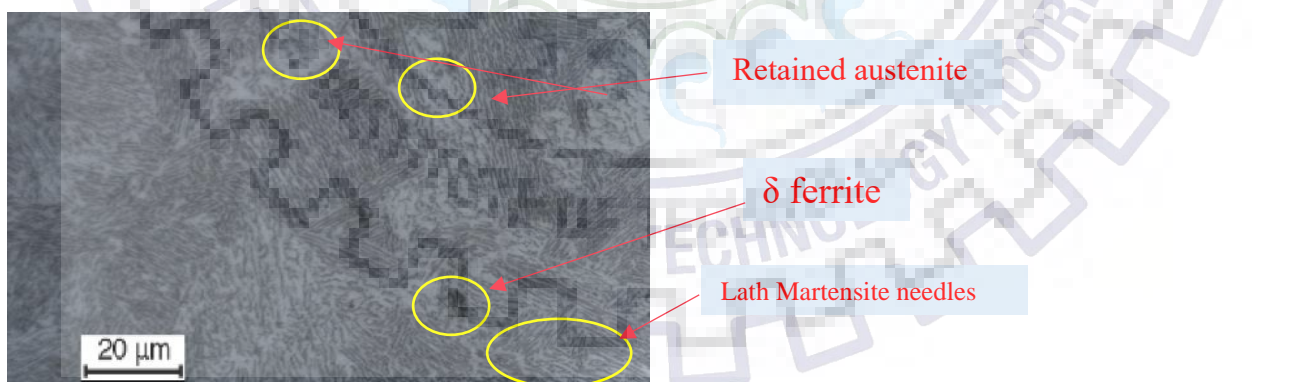


Fig (23b) optical image of 16-5 MSS AISI 431 depicting lath needles and retained austenite

### 5.3 SEM Analysis of bare MSS (ERODED)

The mechanism of material removal in erosion mainly depends on material properties as well as the angle at which the erodent strikes at the surface of the target. Commonly there are two mechanisms reflected to be connected with the removal of material. There are repetitive plastic deformation and cutting. Ductile materials will undergoes mass loss by the process of straight micro cutting or plastic deformation, followed by cutting. While in brittle materials, here energy transfer is associated with repeated particle impacts resulting in a fatigue process. Appearance of specimen, formation of small pits and grooves, which indicates that the material is submitted to plastic deformation. The erosion damage as well as removal of material initiated from its prior austenite grain boundaries and martensite laths. It was observed that there is increase in Ra value as well. The roughness parameters keeps on increasing due to the formation of craters on it with strained material surrounding around them. The worn surface loses the detached particles, eventually micro-cracks grows and joins each other shown in fig (24). After 16 hrs of testing several deep craters, tiny pores fragments had been appeared inside some grains. Bare mss shows ductile to brittle behavior, exhibiting two different modes of material detachment. The first mode was characterized by a great degree of plastic deformation, fatigue and ductile fracture. The second failure mode will be brittle fracture by cleavage mechanisms.

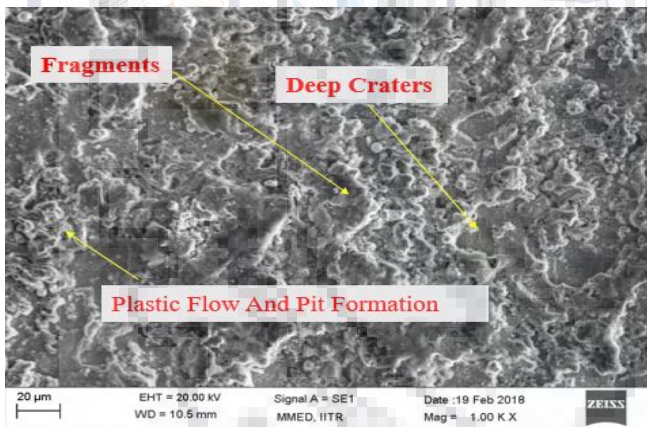


Fig (24a) SEM of nitrided eroded specimen after test at 60 °

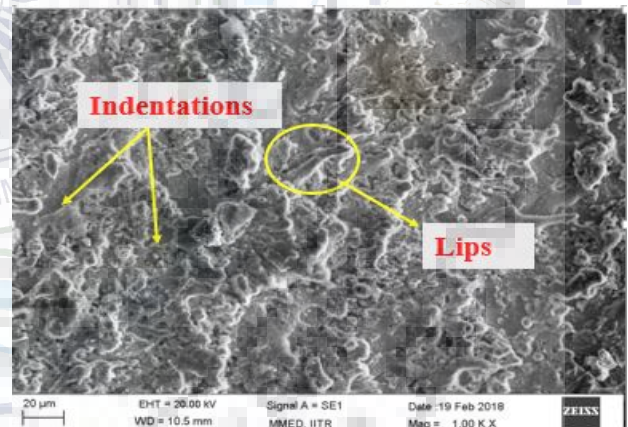


Fig (24b) SEM of nitrided eroded specimen after test at 60 °

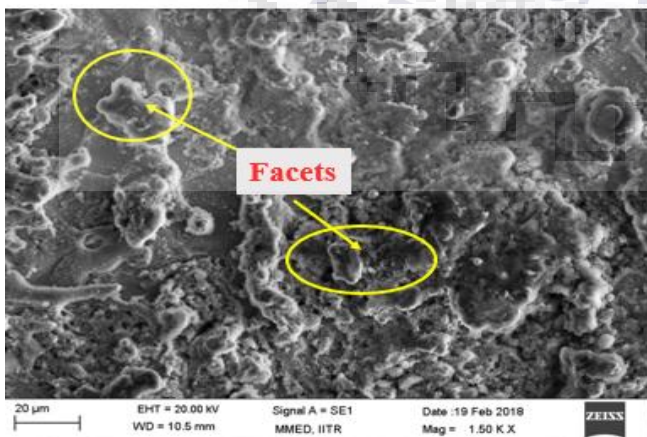


Fig (24c) SEM of nitrided eroded specimen after test at 30 °

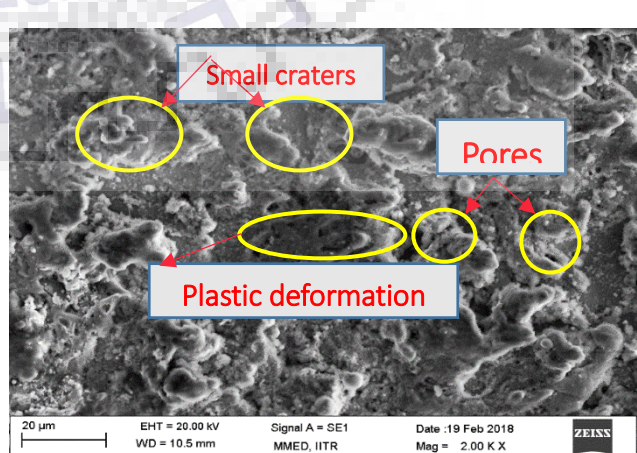


Fig (24d) SEM of nitrided eroded specimen after test at 30 °

#### 5.4 SEM Analysis of MSS (NITRIDED)

**Compound layer** “white structure” is compound zone which is a mixture of both epsilon and gamma-prime structures.

- High internal stresses results from differences in volume growth associated with the formation of each phase.
- The interfaces between the two crystal structures are weak.
- White layer is extremely hard but brittle in nature.
- Layer should be avoided if possible (though no specific guidelines were offered).

**Diffusion zone** beneath this initial region an expanded martensite region forms towards the core shown in fig (25).

- The maximum hardness reaches surface, is around 1021HV

The performance of the nitrided case is controlled by the resistance to elastoplastic deformation given by the expanded martensite.

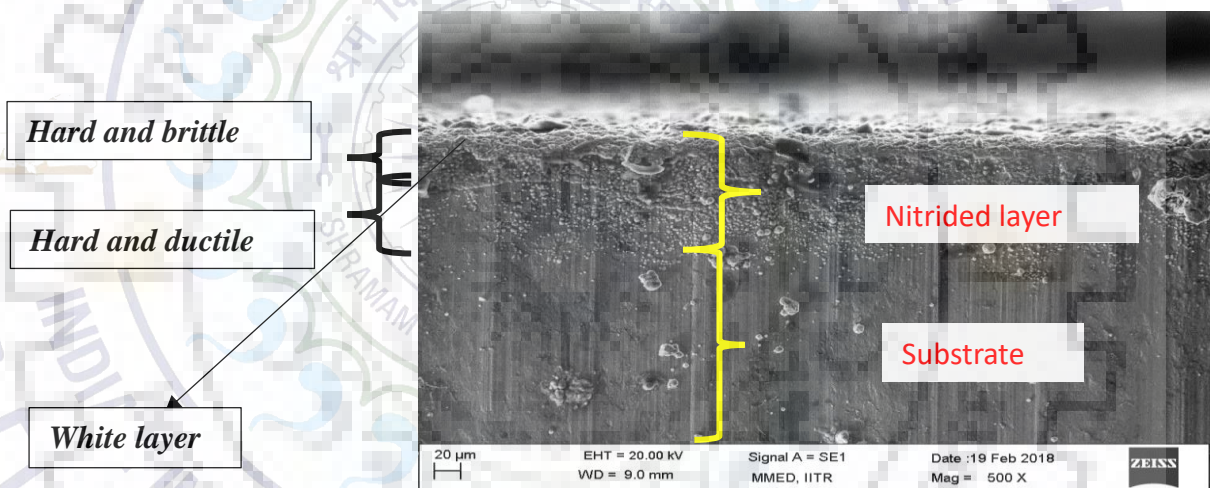


Fig (25 a) SEM of nitrided layer

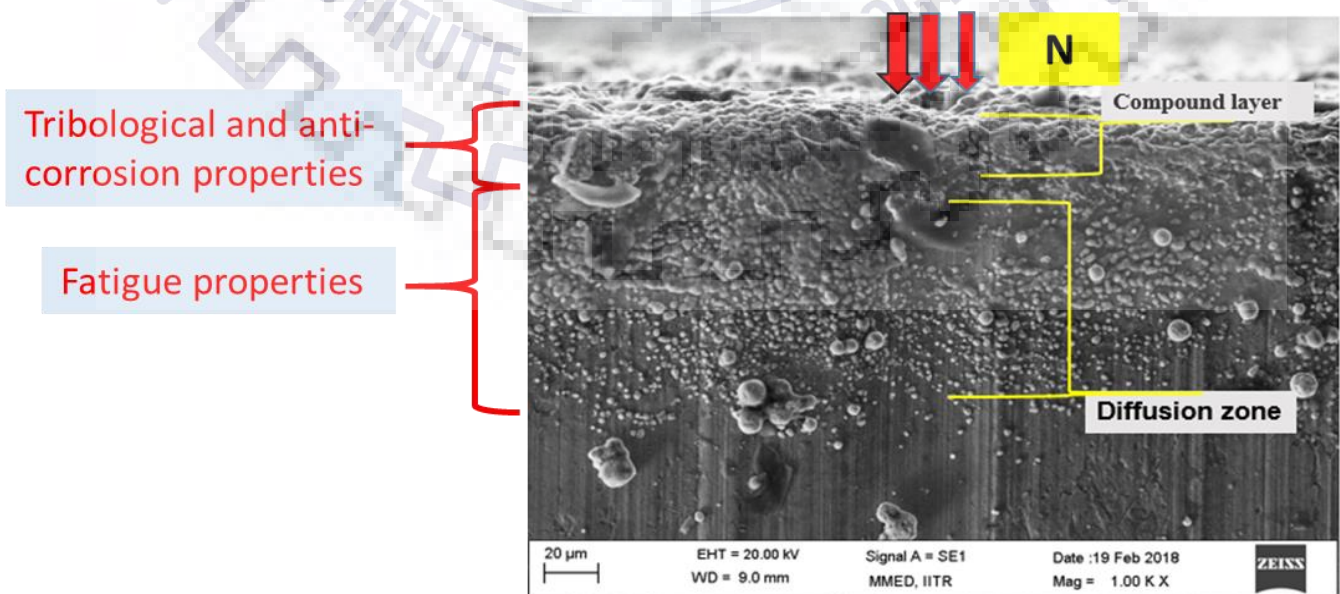


Fig (25 b) SEM of nitrided layer depicting both zones

### 5.5 SEM analysis of nitrided layer

In fig 26 (a) shows Total case depth of coating of Compound layer is of  $5\mu\text{m}$  (very hard and brittle) Diffusion layer is of  $28.6\mu\text{m}$  (hard and ductile in nature) the white layer was identified as a multiphase compound layer of  $\epsilon$  and  $\gamma'$  phases. In fig 26 (b) shows Diffused layer consist of expanded martensite and  $\epsilon$  iron nitride and rest is martensite. Fig 26 (c) At elevated temperature, chromium gets mobile enough to diffuse through the material, form a chemical bond with nitrogen and precipitate in  $\text{Cr}_2\text{N}$  crystallites. one can conclude that the  $\text{Cr}_2\text{N}$  precipitates reduce the corrosion resistance by intergranular sensitization high fluence nitrogen ion implantation in martensite in the temperature up to  $540^\circ\text{C}$  leads to formation of expanded martensite. In fig 26 (d) an anisotropic lattice expansion is also observed.

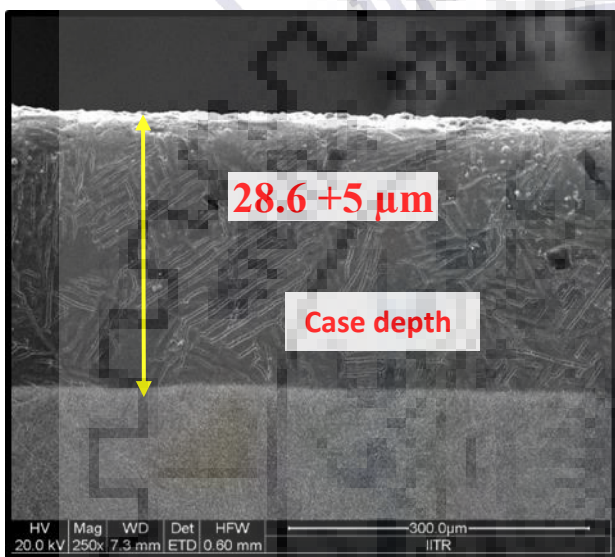


Fig. (26a) Total case depth obtained

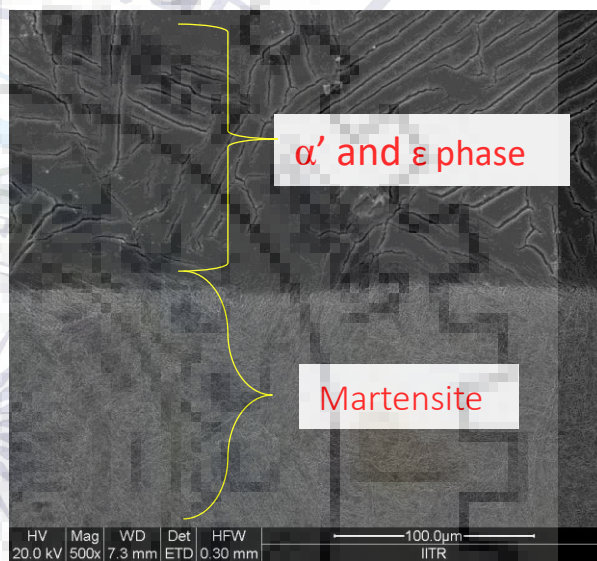


Fig. (26b) SEM depicting diffusion zone and rest MSS

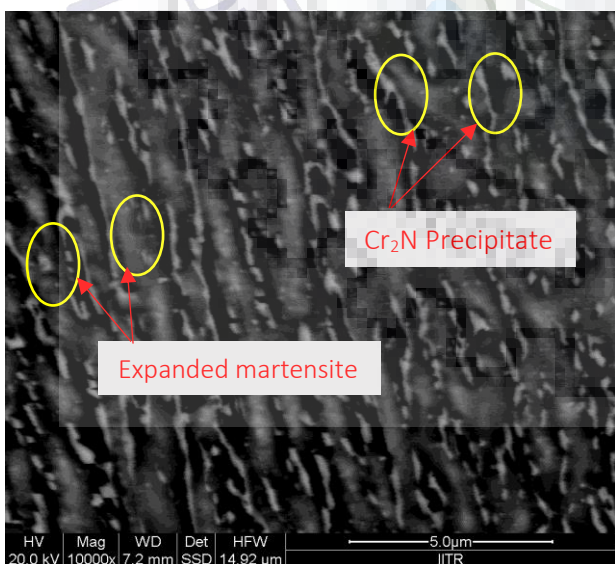


Fig. (26c) Chromium nitrides at grain boundaries

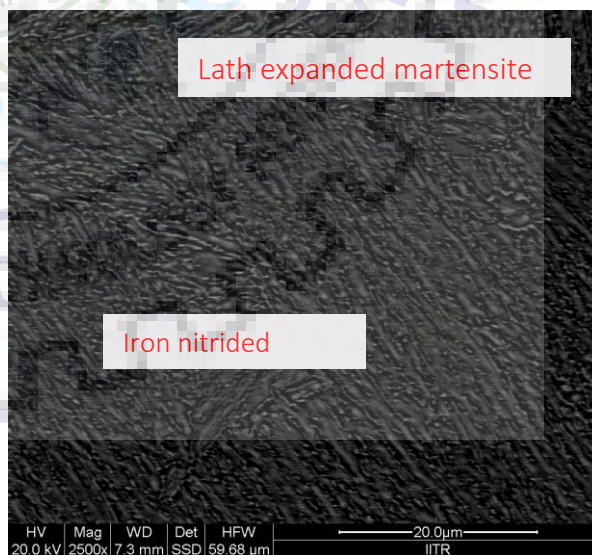


Fig. (26d) Back scattered image of expanded MSS



Precipitates in low carbon martensitic stainless steel during tempering are mainly  $M_{23}C_6$ , where M represents Cr, Mo and Fe. It is reported that the addition of nitrogen delays carbide precipitation and results in disappearance of carbide phase in high nitrogen martensitic stainless steel. Severe precipitation of  $Cr_2N$  along martensitic inter-lath boundaries and within matrix shown in fig (27). Precipitation of rod-like  $Cr_2N$  along martensite lath boundaries and within laths of MSS with N after tempering above  $550^\circ C$  contributes to slight increase in strength and much decrease in toughness compared to the steel without nitrogen actually, the precipitation of  $Cr_2N$  in this



Fig (27a) back scatter image showing Grain boundary

Fig (27b) back scatter mode showing dark Grain boundary

Temperature range is undesirable. However, in order to get more retained austenite to restore. The ductility and toughness, it is necessary to tempering the steel above  $550^\circ C$  at which  $Cr_2N$  would precipitate simultaneously. The chromium can combine with oxygen to form a dense and continuous protective oxide film on the surface, and mitigate the corrosion attack to a certain extent. The nitrogen will dissolve during corrosion process and react with  $H^+$  in solution to form the  $NH_4^+$ . Owing to the cathodic reaction  $[N] + 4H^+ + 3e^- \rightarrow NH_4^+$ , the local pH increase allows to facilitate the re-passivation. However, the beneficial effect of both nitrogen and chromium can be taken only when they are in solid solution and the concentration is high enough, or at least in single phase. Once  $Cr_2N$  forms, the nitrogen and chromium in the solid solution of the nitrided layer will be depleted, which prevents the formation of passivating films on the surface and then deteriorates the corrosion resistance of the stainless steel. The  $450^\circ C$  and  $550^\circ C$  nitriding decrease the corrosion resistance of AISI 431 steel samples only because of the formation of chromium nitride and the depletion of Cr in the solid solution of the nitrided layers. However, the  $350^\circ C$  plasma nitriding treatment prohibits the formation of  $Cr_2N$ , promotes the formation of high chemical stable phases of  $\epsilon-Fe_3N$  and  $\alpha N$  on the nitrided surface, therefore, improves the corrosion resistance of the AISI 431 steel significantly.

## 5.6 SEM Analysis of nitrided eroded

The nitrided specimen surface before and after 4 hrs of testing. During the first 60 min of testing, some tiny pores (1) appeared inside some grains; but, generally speaking, the nitrided specimen surface did not show any significant change and most of the grains remained intact, supporting the fact that the expanded martensite elastically absorbed the shock-waves impact, without plastic deforming. After 105 min, the number of pores inside the grains increased (2) and new pores were nucleated, not only in other grains (3) but also at grain boundaries (4), as can be seen in Fig. 12. Furthermore, it can be seen in Fig. 12 that the damage inside the grain was nucleated at the martensite lath boundaries. The pores nucleation process, along the surface within grains and at grain boundaries, increased with the exposure time, wear particles were detached from the surface, as can be seen for 180 and 300 min of testing time in Figs. 13 and 14, respectively. Moreover, some former pores increased their size and depth, becoming craters (5), particularly those located at martensite laths. It can be inferred that the material removal is due to brittle fracture without plastic deformation. Pores nucleation and growth proceeded and spread over the entire surface till around 600 min of testing, as shown in Fig. 28.

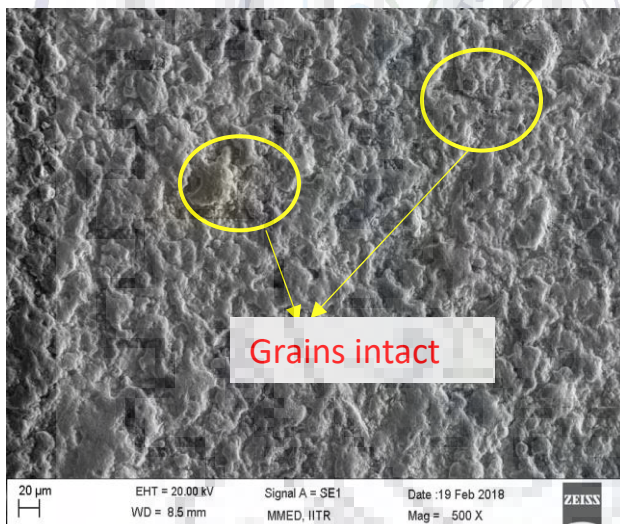


Fig (28a) SEM of nitrided eroded specimen after test at 60°

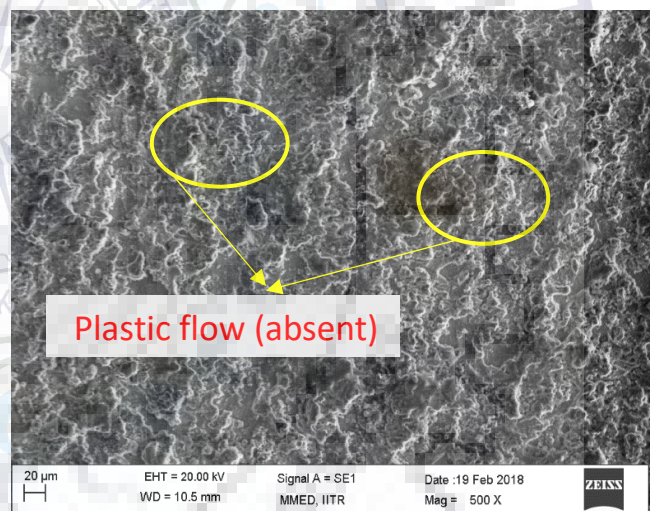


Fig (28b) SEM of nitrided eroded specimen after test at 30°

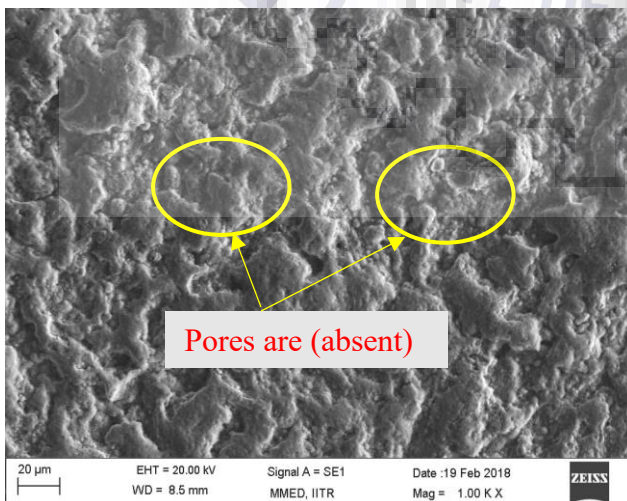


Fig (28c) SEM of nitrided eroded specimen after test at 60°

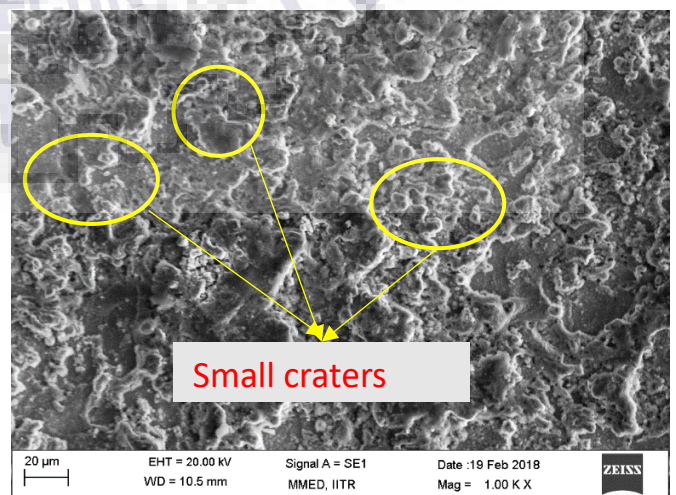


Fig (28d) SEM of nitrided eroded specimen after test at 30°

The original surface was completely removed, but grain Surface did not show any significant change. The grains remained intact, The expanded martensite elastically absorbed the shock-waves impact, without plastic deforming. After 16hrs pores inside the grains are absent not only in other grains but also at grain boundaries. The erosion penetration depth into the nitrided specimen was very low. The wear mechanism remained unchanged. Pores nucleation process, increased with the exposure time, wear particles were detached from the surface former pores increased their size and depth, becoming craters, particularly those located at martensite laths. The material removal is due to brittle fracture without plastic deformation.

Pores nucleation and growth proceeded and spread over the entire surface till around 4hrs of testing, as shown in Fig. 15. The original surface was completely removed, but grain boundaries and craters are still observed. The nitrided case shows a brittle behavior and some cracks (6) nucleated inside the craters. At this time the cumulative mass loss was nearly 0.54 mg, indicating that mass removal occurs in a thin layer at the surface instead of penetrating deeper regions; in other words, the erosion penetration depth into the nitrided specimen was very low. Fig. 16 shows the evolution of the damage at 4 hrs of testing. The wear mechanism remained unchanged along the test. New craters were formed; the nitrided specimen continued losing mass from the craters and by debris detachment from the grains surfaces, due to brittle fracture, without evident plastic deformation.

## 5.7 XRD ANALYSIS

X-ray diffraction patterns for both specimens. As can be seen in Fig. (29 a), the non-nitrided specimen shows typical BCC martensite peaks located at  $2\theta$  angles of 47.81, 78.06 and 99.33. On the other hand, in the nitrided specimen those 3 martensite peaks were broadened and shifted to the left due to the nitrogen gradient along the nitrided case, which produced a different lattice parameter (interplanar spacing) as a consequence of the different nitrogen amounts dissolved at the interstitial sites of the crystal structure. It should be noted that part of the expansion is due to development of compressive stresses in the nitrided case [23]. The peaks located at  $2\theta$  angles of 43.12, 68.11 and 81.60 correspond to a nitrogen supersaturated phase, known as expanded martensite. The  $\alpha'$   $\alpha'$  N (110) expanded martensite region of the X-ray pattern lies between 43.121 and 44.661, as shown in Fig. (29b), indicating a nitrogen gradient inside the nitrided case. In addition to the expanded martensite peaks, the nitrided specimen diffraction pattern shows hexagonal  $\epsilon$ -Fe<sub>24</sub>N<sub>10</sub> iron nitrides peaks structurally similar to  $\epsilon$  Fe<sub>3</sub>N.

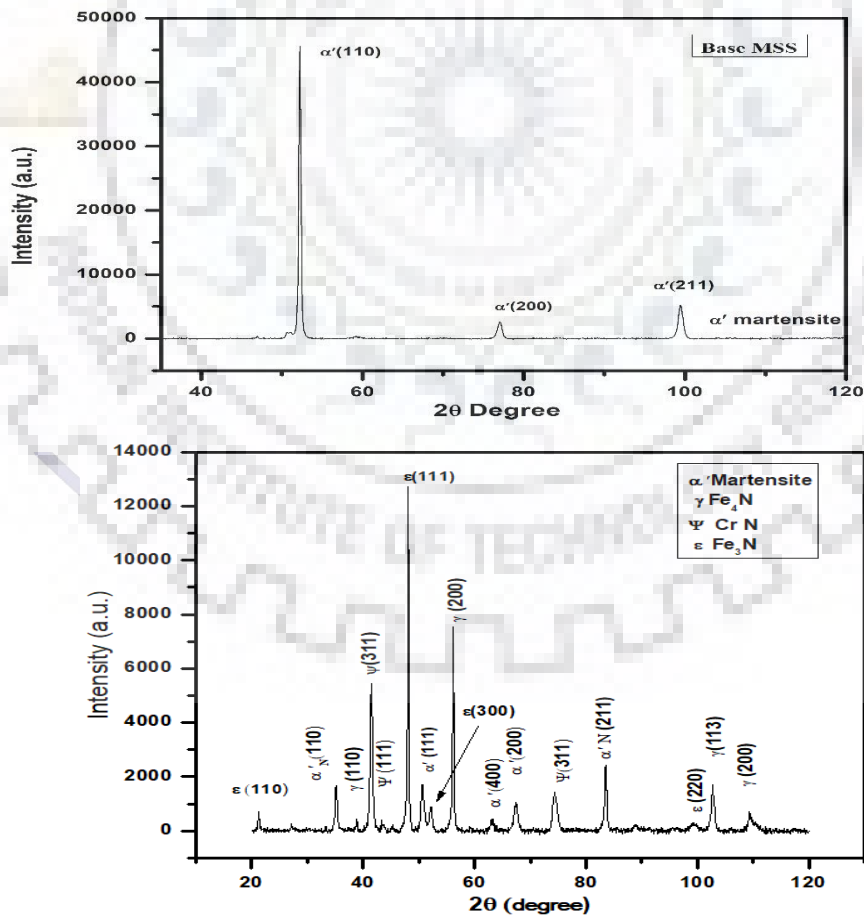


Fig (29b) X-ray diffraction patterns for nitrided specimens.

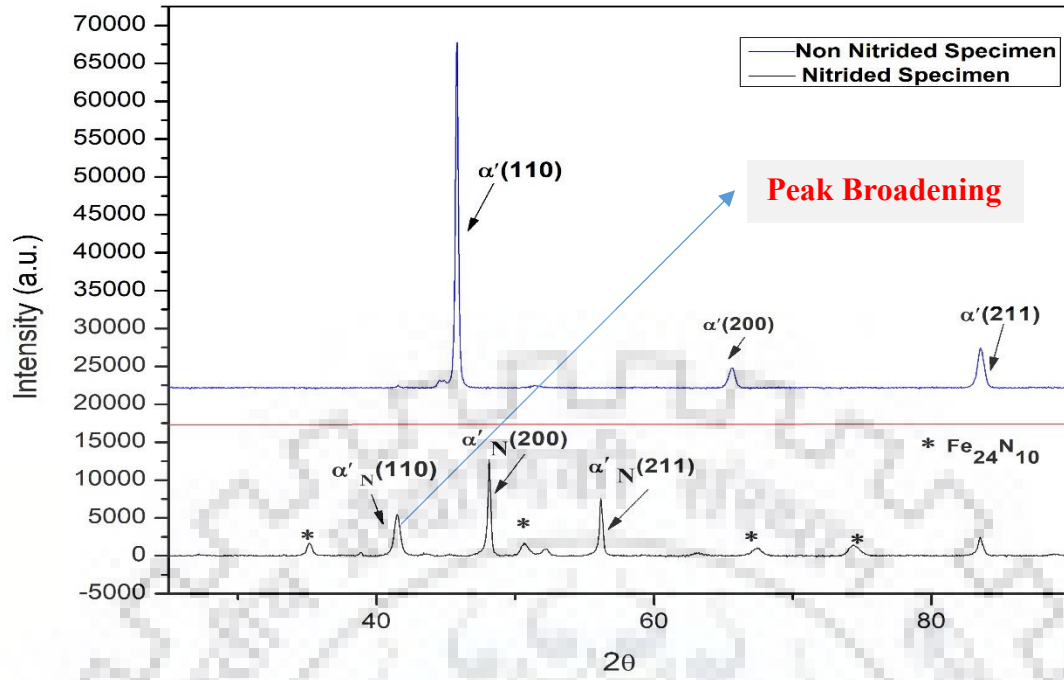


Fig (30 a) X-ray diffraction patterns comparison b/w two

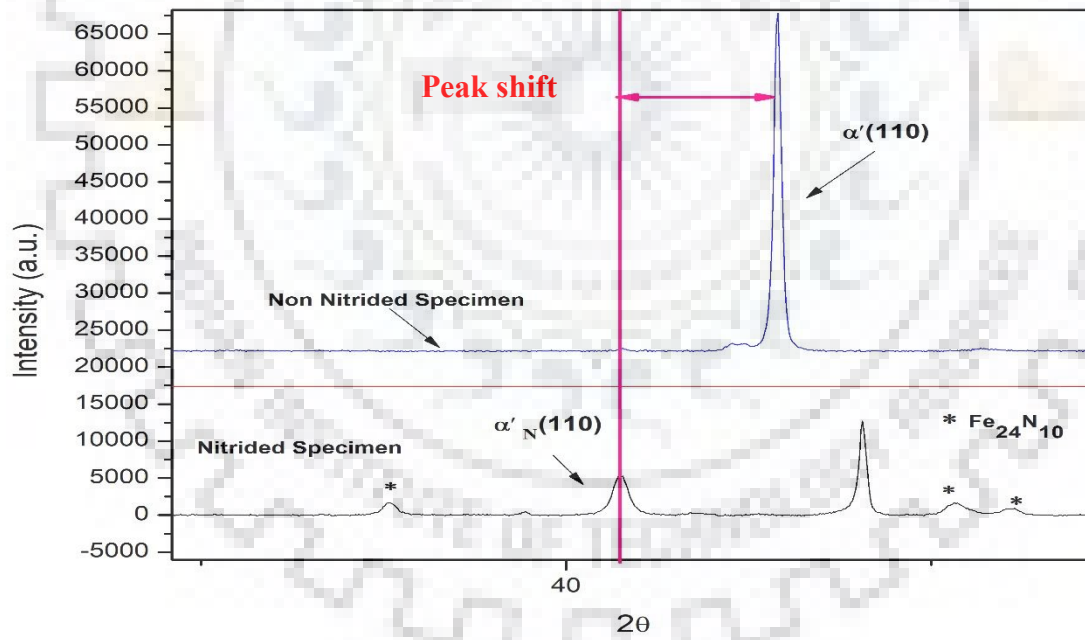


Fig (30 b) X-ray diffraction patterns showing peak shift b/w two specimens.

### 5.8 Weight Loss Plot vs Exposure time

At the initial stage of cavitation, with a high erosion rate (1.2 mg/h), the AISI 410N Rq roughness values remain almost constant (2.5  $\mu\text{m}$ ) from the fourth hour of testing on, implying that the removed mass comes mainly from a maximum depth of 5  $\mu\text{m}$  when this initial nitride containing layer is removed from the sample, only expanded martensite is exposed to the shock-waves produced by cavitation and the erosion rate drops to a lower value of 0.36mg/h shown in fig (31).

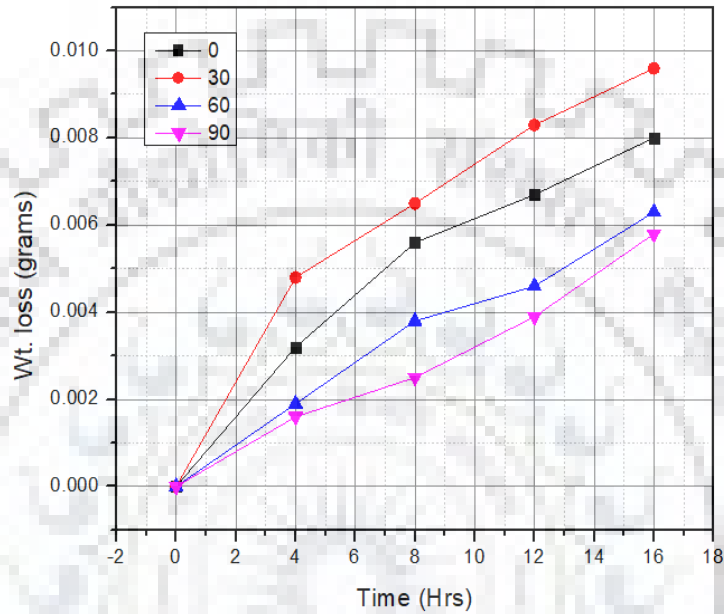


Fig (31a) Wt. loss plot for non nitrided specimen

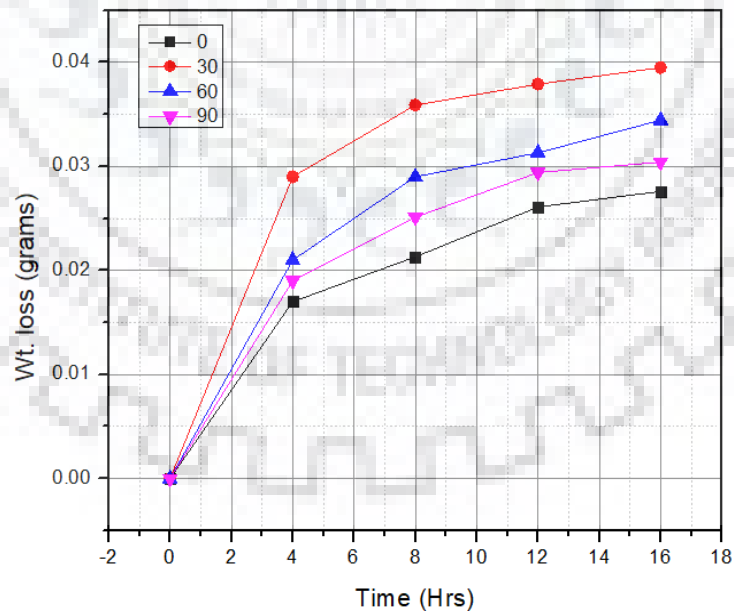


Fig (31b) Wt. loss plot for nitrided specimen

## 5.9 Mass losses and erosion rates

**Cumulative mass losses** variations as a function of exposure time shown in fig 32(a).

After 16 hrs of testing, the non-nitrided specimen lost 39.5 mg and the nitrided specimen lost 9.3 mg. The nitrogen addition decreased 5times the mass loss of the quenched and tempered AISI 431 MSS.

**The erosion rates** were calculated from the slope of the straight line plotted from the 4th hour on accordingly, the erosion rates are 6.9 mg/h and 1.7 mg/h for nitrided and non-nitrided specimens.

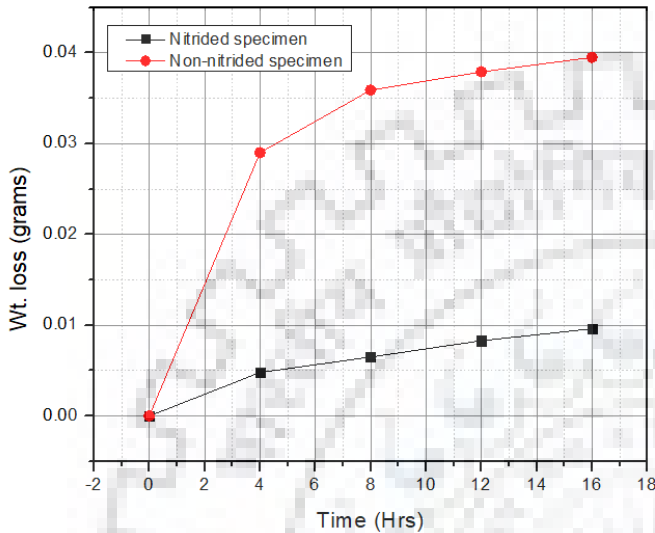


Fig (32a) wt. loss vs exposure time plot

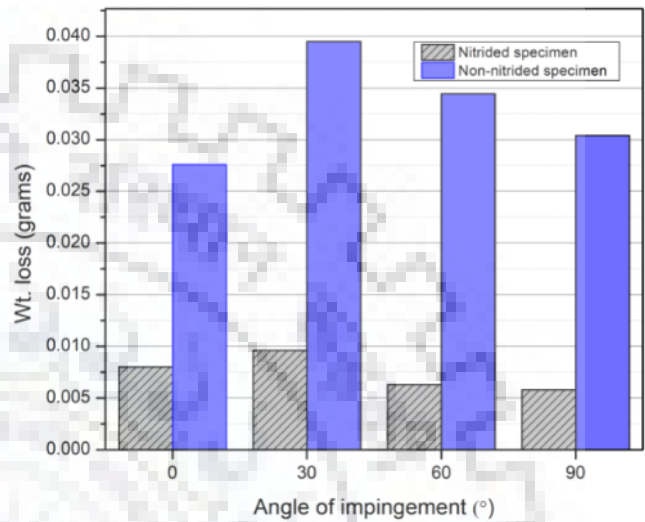


Fig (32b) wt. loss vs angle of impingement

Erosion of a material is dependent upon the angle at which the erodent particles strike the surface of the target. It has been found that maximum erosion rate for a ductile material is at impingement angle of approximately 20–30 and, it decreases at higher angle. Nitrided specimen i.e. AISI431 steel exhibited better performance than the bare AISI 431 steels especially, at angles of impingement of instance, at 90°. This is quite interesting, because the coated layer has very high hardness so, it had shown excellent performance at low angles as well as on high angle of impingement shown in fig 32 (b). This might be due to the transformability of expanded martensite which undergoes repetitive plastic deformation at all angles of impingement.

### 5.10 Roughness Profile and Its Microhardness

It shows the microhardness variation as a function of depth for the nitrided the maximum hardness of 1021 HVN measured on the surface continuously decreases as a consequence of the reduction of nitrogen content with depth, till the hardness of the substrate is achieved shown in fig (33b). The microhardness gradient is very gentle throughout the nitrided case, formation of nitrogen expanded martensite increased the hardness almost 3 times, from for the tempered martensite. While Ra value for nitrided specimen is much lesser than the non nitrided specimen. After 16 hrs of testing results in case of bare MSS is  $1.78\mu\text{m}$  while in nitrided specimen it has reached to the value of  $0.81\mu\text{m}$  shown in fig (33a). This happens because of the wear mechanism take place in the bare MSS. Pores nucleation process, increased with the exposure time, wear particles were detached from the surface, former pores increased their size and depth, becoming craters, particularly those located at martensite laths and thereby the surface roughness parameter goes on increasing.

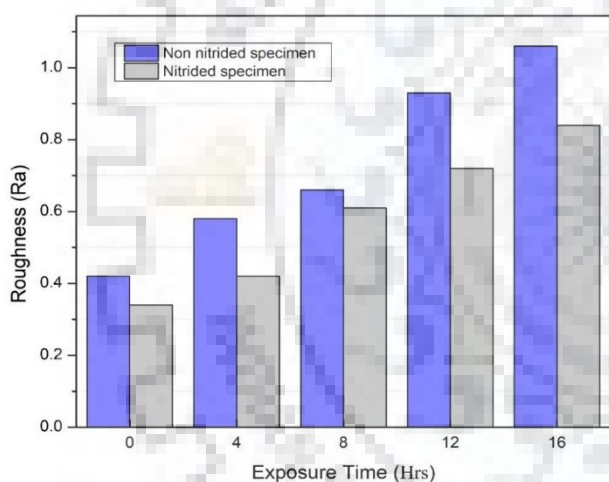


Fig (33a) Surface Roughness Profile

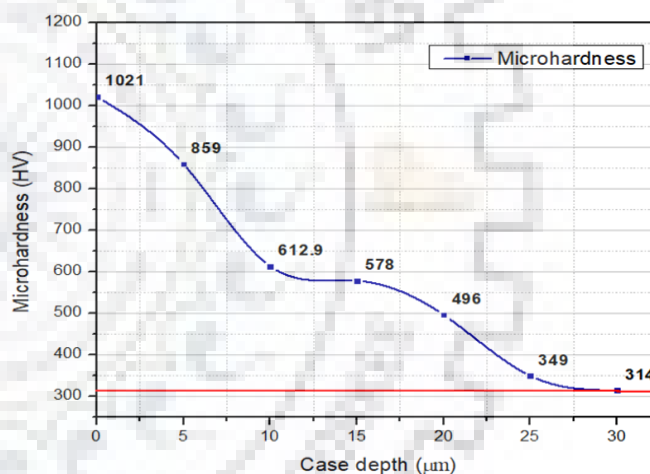
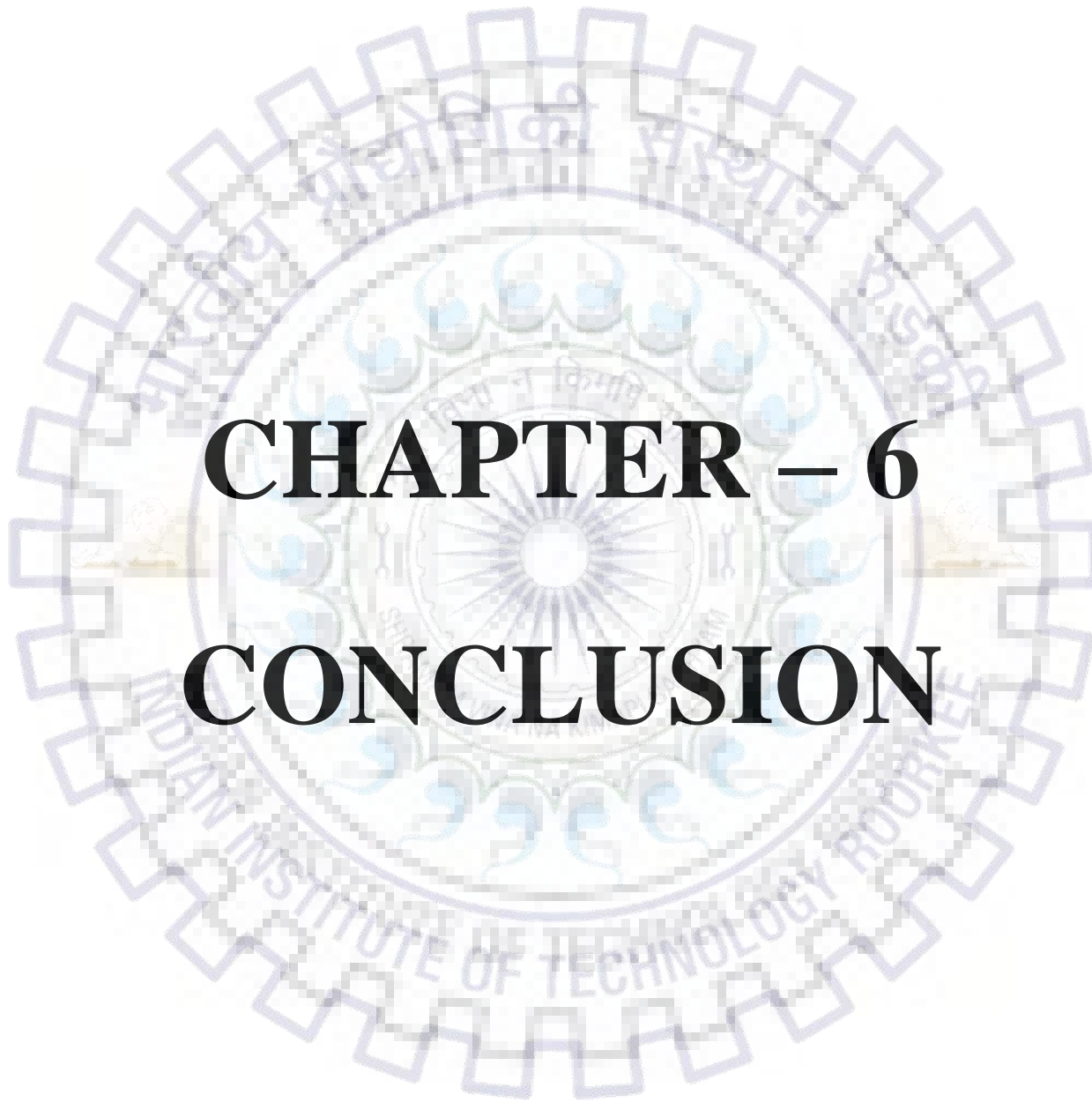


Fig (33b) Case Hardness Profile



The background features a large, faint watermark of the Indian Institute of Technology Rourkee logo. The logo is circular, with a gear-like outer border. Inside the gear, there is a central emblem with a sunburst and a gear. The text "INDIAN INSTITUTE OF TECHNOLOGY ROORKEE" is written around the inner circle of the gear. In the center, there is a Sanskrit motto: "विद्या न विमर्शते" (Vidya na vimarshate).

# **CHAPTER – 6**

# **CONCLUSION**

## 6. CONCLUSION

Nitriding layer on AISI 431 MSS formed by expanded nitrogen supersaturated martensite and hexagonal  $\epsilon$ -Fe<sub>24</sub>N<sub>10</sub>  $\gamma$  and  $\epsilon$  iron nitrides, with maximum hardness of 1021HV measured on top of the nitrided surface. The microhardness measurements on the transverse section of the nitrided specimen is measured by microhardness testing indicated a nitrided case depth around 28.6+5  $\mu\text{m}$  indicating that 5 $\mu\text{m}$  thick compound layer and remaining is diffusion layer. Bare mss shows ductile to brittle behavior, exhibiting two different modes of material detachment. The first mode was characterized by a great degree of plastic deformation, fatigue and ductile fracture. The second failure mode will be brittle fracture by cleavage mechanisms. While in nitrided erosion has been observed that original surface was completely removed, but grain surface did not show any significant change. The grains remained intact, The expanded martensite elastically absorbed the shock-waves impact, without plastic deforming. After 16hrs pores inside the grains are absent not only in other grains but also at grain boundaries. The erosion penetration depth into the nitrided specimen was very low. The wear mechanism remained unchanged. Pores nucleation process, increased with the exposure time, wear particles were detached from the surface former pores increased their size and depth, becoming craters, particularly those located at martensite laths. The material removal is due to brittle fracture without plastic deformation. High nitrogen martensitic stainless steel will undergoes severe precipitation of Cr<sub>2</sub>N along martensitic inter-lath boundaries and within matrix. Precipitation of rod-like Cr<sub>2</sub>N along martensite lath boundaries and within laths of MSS with N after tempering above 550°C contributes to slight increase in strength and much decrease in toughness compared to the steel without nitrogen actually. Once Cr<sub>2</sub>N forms, the nitrogen and chromium in the solid solution of the nitrided layer will be depleted, which prevents the formation of passivating films on the surface and then deteriorates the corrosion resistance of the stainless steel. After 16h of testing, the non-nitrided specimen lost nearly 39.5 mg and the nitrided specimen lost just 9.3 mg. The Nitrided nitrogen supersaturated expanded martensite decreased 5 times the mass loss compared to the quenched and tempered AISI410 stainless steel. The erosion rates were 6.9 mg/h and 1.7 mg/h for the nitrided and non-nitrided specimens, respectively.

## REFERENCES

- [1] D. Whale and D. Hart, A Review of Cavitation-Erosion-resistant Weld Surfacing for Hydro Turbines, Proceedings of the Asian-Pacific Welding Conference (Auckland, New Zealand), 1996
- [2] G.I. Nikitenko, Studies to Reduce Cavitation Erosion of the Impellers in the Hydro Turbines at the Sayano-Shushenskoe Hydroelectric Plant, *Hydrotech. Constr.*, 1998,32(9), p 570–573
- [3] M.G. Fontana, *Corrosion Engineering*, McGraw Hill, Singapore, 1986,p 104
- [4] W.S. Lamb, *Cavitation and Aeration in Hydraulic Systems*, BHR Group, Bedfordshire, 1987, p 114
- [5] C.M. Hansson and I.L.H. Hansson, *ASM Handbook: Friction, Lubr.Wear Technol.*, 1992, 18, p 214–220
- [6] C.M. Preece, *Treatise on Materials Science and Technology, Volume16, Erosion*, Academic Press Inc., New York, 1979, p 249–308
- [7] G.W. Stachowiak, A.W. Batchelor, Abrasive, erosive and cavitation wear, in: *Engineering Tribology*, Elsevier, 1993, pp. 501e551.
- [8] K.J. Stein, B.S. Schorr, A.R. Marder, Erosion of Thermal Spray MCr–Cr<sub>3</sub>C<sub>2</sub> cermet coatings, *Wear* 224 (1999) 153–159.
- [9] J.A. Browning, Viewing the future of high velocity oxy fuel (HVOF) and high velocity Air fuel (HVOF), *J. Thermal Spray Technol.* 8 (3)(1999) 351–356.
- [10] D.A. Stewart, P.H. Shipway, D.G. McCartney, Influence of heat treatment on the Abrasive wear behaviour of HVOF sprayed WC–CO coating, *Surface Coating Technol.* 105 (1998) 13–24.
- [11] H.M. Hawthorne, B. Arsenault, J.P. Immarigeon, J.G. Lagouse, V.R. Parameswaram, Comparison of slurry and dry erosion behavior of some HVOF thermal sprayed coatings, *Wear* 225–229 (1999) 825–834

- [12] B.K. Pant, Vivek Arya, and B.S. Mann, Enhanced Droplet Erosion Resistance of Laser Treated Nano Structured TWAS and Plasma Ion-Nitro carburized Coatings for High Rating Steam Turbine Components, *J. Therm. Spray Technol.*, 2010, 19(5), p 884–892
- [13] C.T. Kwok, K.H. Lo, F.T. Cheng, and H.C. Man, Effect of Processing Conditions on the Corrosion Performance of Laser Surface-Melted AISI 440C Martensitic Stainless Steel, *Surf. Coat. Technol.*, 2003, 166, p 221–230
- [14] C.T. Kwok, H.C. Man, and F.T. Cheng, Cavitation Erosion and Pitting Corrosion Behavior of Laser Surface-Melted Martensitic Stainless Steel UNS S42000, *Surf. Coat. Technol.*, 2000, 126, p 238–255
- [15] C. Blawert, B. L. Mordike, U. Rensch, G. Schreiber & H. Oettel Nitriding Response of Chromium Containing Ferritic Steels on Plasma Immersion Ion Implantation at Elevated Temperature
- [16] Yun-tao Xi □ Dao-xin Liu, Dong Han Improvement of corrosion and wear resistances of AISI 420 martensitic stainless steel using plasma nitriding at low temperature.
- [17] A.N. Allensteina, R.P. Cardoso, Strong evidences of tempered martensite-to-nitrogen-expanded austenite transformation in CA-6NM steel.
- [18] X.P. Maa, L.J. Wang Effect of N on microstructure and mechanical properties of 16Cr5Ni1Mo martensitic stainless steel.
- [19] L.A. Espitia a,n, L.Varela a, Cavitation erosion resistance of low temperature plasma nitrided martensitic stainless steel.
- [20] J.F. Santa, J.C. Baena, Slurry erosion of thermal spray coatings and stainless steels for hydraulic machinery, *Wear* 263 (2007) 258–264
- [21] Y. Iwabuchi and S. Sawada Metallurgical Characteristics of a Large Hydraulic Runner Casting of Type 13Cr-Ni Stainless Steel 1982, pp. 332-354
- [22] D. Manova a,\* , G. Thorwarth b, S. Ma'ndl a, Variable lattice expansion in martensitic stainless steel after nitrogen ion implantation 242 (2006) 285–288

- [23] C. A. Figueroaa, F. Alvarez, Z. Zhang, G. A. Collins, and K. T. Short Structural modifications and corrosion behavior of martensitic stainless steel nitrided by plasma immersion ion implantation (21 June 2005 )
- [24] A. Leylanda, D. B. Lewis”, P. R. Stevenson~’and A. Matthews Low temperature plasma diffusion treatment of stainless steels for improved wear resistance, 62 (1993) 608—617
- [25] I. Alphonsa, A. Chainani, P. M. Raole, B. Ganguli, and P. I. John, Surf. Coat. Technol. **150**, 263 (2002).
- [26] 12G. A. Collins, R. Hutchings, K. T. Short, and J. Tendys, Surf. Coat. Technol. **103–104**, 212 (1998)

